AERODYNAMIC PARAMETER ESTIMATION OF A MISSILE
IN CLOSED LOOP CONTROL AND VALIDATION WITH FLIGHT DATA

A THESIS SUBMITTED TO
THE GRADUATE SCHOOL OF NATURAL AND APPLIED SCIENCES
OF
THE MIDDLE EAST TECHNICAL UNIVERSITY

BY

GÜNEŞ AYDIN

IN PARTIAL FULFILLMENT OF THE REQUIREMENTS
FOR
THE DEGREE MASTER OF SCIENCE
IN
AEROSPACE ENGINEERING

SEPTEMBER 2012

Approval of the thesis:

**AERODYNAMIC PARAMETER ESTIMATION OF A MISSILE
IN CLOSED LOOP CONTROL AND VALIDATION WITH FLIGHT DATA**

submitted by **GÜNEŞ AYDIN** in partial fulfillment of the requirements for the degree of **Master of Science in Aerospace Engineering Department, Middle East Technical University** by,

Prof. Dr. Canan Özgen                           _____
Dean, Graduate School of **Natural and Applied Sciences**

Prof. Dr. Ozan Tekinalp                           _____
Head of Department, **Aerospace Engineering**

Asst. Prof. Dr. Ali Türker Kutay                   _____
Supervisor, **Aerospace Engineering Dept., METU**

**Examining Committee Members:**

Prof. Dr. Ozan Tekinalp                           _____
Aerospace Engineering Dept., METU

Asst. Prof. Dr. Ali Türker Kutay                   _____
Aerospace Engineering Dept., METU

Asst. Prof. Dr. İlkay Yavrucuk                    _____
Aerospace Engineering Dept., METU

Assoc. Prof. Dr. Tayfun Çimen                   _____
Engineering Development Directorate,
Roketsan Missile Industries Inc.

Haydar Tolga Avcıoğlu                          _____
Engineering Development Directorate,
Roketsan Missile Industries Inc.

**Date:**         _____

I hereby declare that all information in this document has been obtained and presented in accordance with academic rules and ethical conduct. I also declare that, as required by these rules and conduct, I have fully cited and referenced all material results that are not original to this work.

Name, Last name :    Güneş Aydın

Signature            :

# ABSTRACT

AERODYNAMIC PARAMETER ESTIMATION OF A MISSILE
IN CLOSED LOOP CONTROL AND VALIDATION WITH FLIGHT DATA

Aydın, Güneş

M.Sc., Department of Aerospace Engineering

Supervisor Asst. Prof. Dr. Ali Türker Kutay

September 2012, 80 pages

Aerodynamic parameter estimation from closed loop data has been developed as another research area since control and stability augmentation systems have been mandatory for aircrafts. This thesis focuses on aerodynamic parameter estimation of an air to ground missile from closed loop data using separate surface excitations. A design procedure is proposed for designing separate surface excitations. The effect of excitations signals to the system is also analyzed by examining autopilot disturbance rejection performance. Aerodynamic parameters are estimated using two different estimation techniques which are ordinary least squares and complex linear regression. The results are compared with each other and with the aerodynamic database. An application of the studied techniques to a real system is also given to validate that they are directly applicable to real life.

Keywords: Open Loop Parameter Estimation from Closed Loop Data, Input Design, Ordinary Least Squares, Complex Linear Regression

# ÖZ

KAPALI DÖNGÜ KONTROLÜNDE BİR FÜZENİN
AERODİNAMİK PARAMETRE TAHMİNİ VE UÇUŞ VERİSİYLE GEÇERLEME

Aydın, Güneş

Yüksek Lisans, Havacılık ve Uzay Mühendisliği Bölümü

Tez Yöneticisi: Yrd. Doç. Dr. Ali Türker Kutay

Eylül 2012, 80 sayfa

Hava araçlarında, kapalı döngü sistem verilerinden aerodinamik parametre tahmini kontrol ve kararlılık sistemlerinin kullanılmasıyla ortaya çıkmış bir araştırma alanıdır. Bu tezde ayrık kanatçık komutları kullanılarak kapalı döngü kontrolünde, havadan karaya bir füze sistemin aerodinamik parametrelerinin tahminini incelenmiştir. Çalışma kapsamında ayrık kanatçık komutları için sistematik bir tasarım yöntemi önerilmiştir. Kullanılan ayrık kanatçık komutlarının sisteme olan bozucu etkisi incelenmiştir. Aerodinamik parametrelerin tahmini için sıradan en küçük karaler yöntemi ve karmaşık doğrusal regresyon olmak üzere iki farklı tahmin yöntemi kullanılmıştır. Sonuçlar birbirleriyle ve aerodinamik veritabanı ile karşılaştırılmıştır. Tez kapsamında kullanılan yöntemler gerçek bir sisteme uygulanarak bu çalışmaların gerçek hayata doğrudan uygulanabilirliği kanıtlanmıştır.

Anahtar Kelimeler: Kapalı Döngü Veriden Açık Döngü Parametre Tahmini, Girdi Tasarımı, Sıradan En Küçük Kareler Yöntemi, Karmaşık Doğrusal Regresyon

To My Parents

# ACKNOWLEDGMENTS

# TABLE OF CONTENTS

# LIST OF TABLES

TABLES

# LIST OF FIGURES

FIGURES

# LIST OF ABBREVIATIONS

$p$      Body roll rate

$q$      Body pitch rate

$r$      Body yaw rate

$\phi$      Roll angle

$\theta$      Pitch angle

$\psi$      Yaw angle

$a_x$      Acceleration in body x-axis

$a_y$      Acceleration in body y-axis

$a_z$      Acceleration in body z-axis

$u$      Velocity in body x-axis

$v$      Velocity in body y-axis

$w$      Velocity in body z-axis

$V$      Total velocity

$V_{x_e}$      x component of total velocity in earth axis

$V_{y_e}$      y component of total velocity in earth axis

$V_{z_e}$      z component of total velocity in earth axis

$x_e$      x position in earth axis

$y_e$      y position in earth axis

$z_e$      z position of total velocity in earth axis

$h$      Altitude in earth frame axis

$a_n$      Acceleration command in body x-axis

$\delta_e$      Elevator command

$\delta_r$      Rudder command

$\delta_a$      Aileron command

$a_{sound}$      Speed of sound

| | |
|---|---|
| $\rho$ | Air density |
| $g$ | Gravitational constant |
| $g_x$ | x component of gravitational force in body axis |
| $g_y$ | y component of gravitational force in body axis |
| $g_z$ | z component of gravitational force in body axis |
| $w_n$ | Natural frequency |
| $X$ | x component of aerodynamic force in body axis |
| $Y$ | y component of aerodynamic force in body axis |
| $Z$ | z component of aerodynamic force in body axis |
| $L$ | Aerodynamic roll moment |
| $M$ | Aerodynamic pitch moment |
| $N$ | Aerodynamic yaw moment |
| $T$ | Total thrust |
| $T_x$ | x component of thrust in body axis |
| $T_y$ | x component of thrust in body axis |
| $T_z$ | x component of thrust in body axis |
| $c.g.$ | Center of gravity |
| $m$ | Mass |
| $I$ | Moment of inertia |
| $l$ | Reference length |
| $S$ | Reference area |
| $\alpha$ | Angle of attack |
| $\beta$ | Angle of sideslip |
| $Q$ | Dynamic pressure |
| $L_{EB}$ | Body frame to Earth frame transformation matrix |
| $C_x$ | Nondimensional aerodynamic force coefficient in body x-axis |
| $C_y$ | Nondimensional aerodynamic force coefficient in body y-axis |
| $C_z$ | Nondimensional aerodynamic force coefficient in body z-axis |

$C_N$     Nondimensional aerodynamic force coefficient in minus body z-axis

$C_l$     Nondimensional aerodynamic roll moment coefficient in body x-axis

$C_m$     Nondimensional aerodynamic pitch moment coefficient in body y-axis

$C_n$     Nondimensional aerodynamic yaw moment coefficient in body z-axis

# CHAPTER 1

# INTRODUCTION

## 1.1 Focus of the Study

System identification activity can be explained as developing mathematical models for physical systems based on imperfect observations [1]. In this large research area aerodynamic parameter estimation is an important study field especially for air vehicles. The aerodynamic parameter estimation results are widely used for several purposes such as verifying and improving computational and wind-tunnel test results, developing flight simulations in large flight regimes, and investigating stability and control impact of airframe modifications.

As the complexity of aircrafts increases automatic control systems like stability augmentation systems become mandatory. This necessity brings new challenges in the parameter estimation field such as open loop parameter estimation from closed loop data.

Aerodynamic parameter estimation of an air vehicle from closed loop system is studied in this thesis with the focus of designing excitation signals. In addition to that different estimation techniques are compared. Finally the methodology and techniques studied in this work are validated with real flight data.

## 1.2 Review of Literature

Aerodynamic parameter estimation has been studied since early powered flight. From that period estimation of aerodynamic parameters has been studied by various

researchers. The general methodology of system identification can be summarized by "Quad-M" [3]. The four "M" indicates **M**otion, **M**easurement, **M**odel and **M**ethod. Motion of the aircraft addresses that one should design the input which excites all the modes of the aircraft. After excitation part the motion of the aircraft should be measured with high accuracy. In other words sensor filtering and instrumentation of the aircraft is another important issue in identification process. A mathematical model which identifies aircraft motion is the next step in the process. Finally selecting suitable estimation technique ends system identification process. The systematic treatment of this methodology has been applied by various authors. The applications can be found in the works Hamel [4], Mulder [5], Maine and Iliff [6], and Klein [7].

In the late 1960s and early 1970s digital computers made a dramatic impact to the system identification field. In that period various estimation techniques were developed and applied. These techniques are mostly off-line methods. In other words they require post-flight analysis of flight data. These post-process estimation techniques are namely statistical methods. The Ordinary Least Squares method and Maximum Likelihood Method are widely used among them. The broad overview of these techniques can be found in the works of Klein, Morelli and Jategaonkar [1, 2].

As the need for agility and maneuver capability increased over the years, aircraft are designed to be inherently unstable. Unstable aircrafts require automatic control systems for safe operation. Therefore parameter estimation for such aircrafts needs to be performed during closed-loop operation and this brings some new challenges. Some of these challenges are addressed by Klein [8] and Klein and Murphy [9]. In the work of Klein [8] and Klein and Murphy [9], a system identification methodology applied to high performance aircraft was introduced. In the methodology optimal input design, data collinearity analysis and biased estimation techniques for highly collinear data were examined. It can be seen in these works that highly maneuverable, inherently unstable and highly augmented aircrafts require high sophistication in aircraft identification methodology [9].

The references mentioned in the previous paragraphs and many other studies in the literature show that open loop aerodynamic parameter estimation in the presence of data collinearity is a very rough challenge. However, reducing data collinearity can be a solution to this problem. This solution can be realized by applying separate surface excitations (SSE) to the closed loop system. One of the applications of this method can be seen in the work of Weiss, Friehmelt, Plaetschke and Rohlf [10]. In this work aerodynamic parameter estimation of the X-31A experimental aircraft was conducted. The quality of the identification results, especially in the high-angle-of-attack regime, suffered from high correlations between the aircraft controls and states as well as from insufficient sideslip excitation [10]. The cause of the correlation problem is the control system of the unstable aircraft. The correleation was decreased by applying SSE to the aircraft. Three side views of the X-31 experimental aircraft are shown in Figure 1-1.
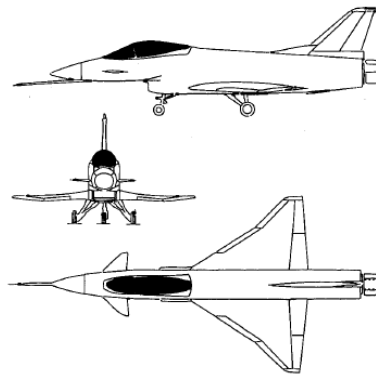


**Figure 1-1 Three side views of the X-31, [10]**

In the result of this work, it was shown that aerodynamic parameter from SSE are close to the predictions and have small uncertainty levels [10]. On the other hand estimation results from pilot maneuvers resulted in large scatter and error bounds [10], due to high correlation. These differences between results are shown in Figure 1-2. Inputs applied by the pilot are suppressed by feedback control and the estimation results aren't good enough due to high correlation between the inputs and outputs

caused by feedback control. Whereas separate surface inputs generated by a "Flutter Box" decreased correlation level between aircrafts controls and states.
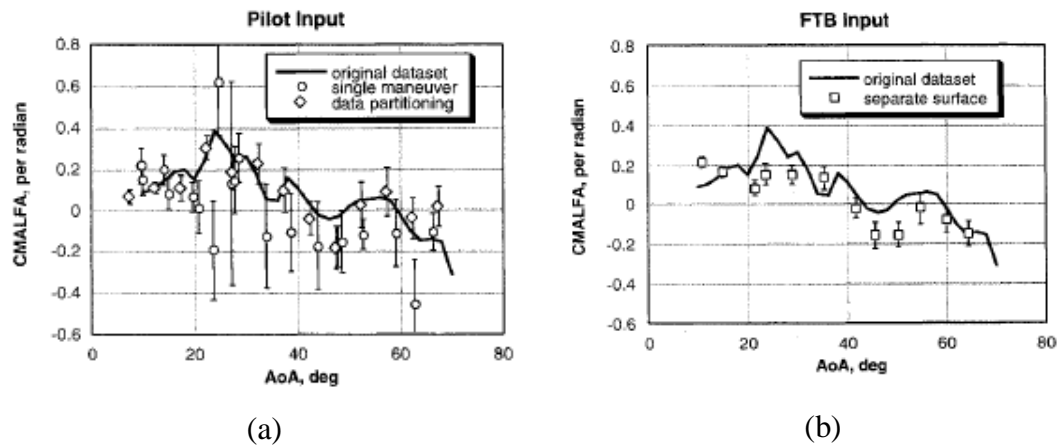


**Figure 1-2 Estimation results, (a) Pilot Input, (b) Separate Surface Input, [10]**

Another implementation can be found in the work of Moes, Smith and Morelli [11]. In this work stability and control derivatives are estimated near real time for Intelligent Flight Control System developed by NASA. The control system is used in F-15B aircraft that is modified by adding a set of canards [11]. The airplane has five pairs of control surfaces which are elevators, canards, ailerons, trailing-edge flaps and rudders. For the nominal flight control system, pilot stick and rudder inputs result in high correlation between the symmetric canard and angle of attack ($\alpha$), rudder and differential canard, and differential stabilator and aileron [11]. Three side views of the X-31 experimental aircraft are shown in Figure 1-3.
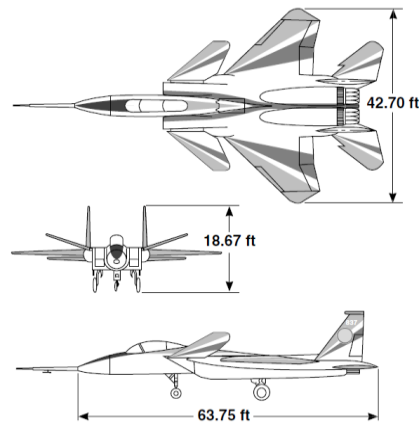
**Figure 1-3 Three side view of the F-15B, [11]**

The main purpose of the intelligent control system is to modify control laws under failure conditions such as actuator failures or wing damage. The control systems need near real-time estimation of aerodynamic stability and control derivatives. These estimated derivatives are supplied to an adaptive online-learning neural network [11]. A schematic diagram of the developed control system is shown in Figure 1-4.
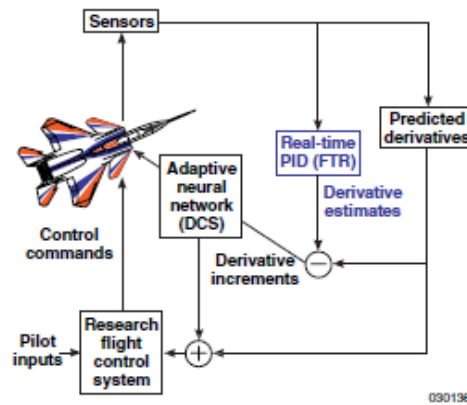


**Figure 1-4 Schematic of the real-time Parameter Identification (PID), [11]**

In a modern aircraft control system a simple stick or rudder input could result in multiple control-surface actuations that are highly correlated in time and shape [11]. In order to reduce data correlation estimation process was done by using SSE.

Application of SSE is a complicated task. Because of the need for rapid derivative identification, after some unknown damage all control surfaces need to be excited simultaneously but still independently from each other [11]. To meet this requirement input signals were desiged as sinusoidal signals at different frequencies. This work shows that SSE provides excellent derivative estimation in the longitudinal plane.

The usage area of SSE was widened as the need for parameter estimation was increased for augmented systems. There were various works on multiple input designs and near real-time frequency domain estimation. Some of these works can be found in references [12], [13], [14] and [15].

## 1.3 Contribution of the Thesis

This thesis has the following contributions to the system identification field

An input design procedure is presented for closed loop aerodynamic parameter estimation of an air to ground missile. The collinearity problem due to closed loop system is examined. Different excitation inputs are studied. It is shown that as the collinearity in the closed loop data reduces the open loop estimation techniques can be easily applied to closed loop data.

Two different estimation techniques are applied. One of these techniques is a time domain technique and the other is a frequency domain technique. Their results and performance are compared with each other and with the aerodynamic database of the missile.

The techniques studied in the thesis are also applied to a real system which is an air to ground missile. The missile flight computer was recoded in order to apply pre-designed surface excitations to the system. SSE is selected to reduce collinearity of the measured data. The results from real flight data are also compared with the

results of 6-DOF simulation to validate simulation results. It is shown that SSE technique works well for reducing data collinearity in the closed loop data and consequently estimation results can be improved significantly.

## 1.4 Structure of the Thesis

The outline of the remaining chapters of the thesis is as follows;

In Chapter 2, the characteristics of the AGM-84A Harpoon missile and 6-DOF simulation developed for this thesis are presented. The equations of motion and aerodynamic model equations are also presented here. Simulation results are discussed at the end of the chapter.

In Chapter 3, parameter estimation methodology and the estimation techniques are examined. Input design strategy to collect closed loop data and parameter estimation results with two different estimation techniques are presented. The results are compared with each other and with the aerodynamic database. The parameter estimation results from real flight data are also presented here.

And finally in Chapter 4 conclusion and future works are discussed.

# CHAPTER 2

# 6-DOF MISSILE FLIGHT SIMULATION

The estimation process studied in this thesis is done using data generated from 6-DOF missile flight simulation. In the modeling process Harpoon Missile (AGM-84A, Air to Ground Missile-84 Variant A) system is selected as a baseline configuration. The main purpose of selecting of a cruise missile as a reference model for flight simulation is the flight regime of the cruise missiles which are very close to conventional aircraft. So the methodologies and techniques studied here can be easily used for aircraft flying at similar flight conditions.

## 2.1 AGM-84A Harpoon Missile

The Harpoon Missile is an all-weather, over-the-horizon, anti-ship missile system. It can be launched from air and ship platforms, submarines and land-based coastal defense batteries [16]. It was firstly produced by McDonnell Douglas which was later merged with Boeing at the late 1990s [16, 17]. The missile was first introduced in 1977, and in 1979 the air-launched version was deployed on the Navy's P-3C Orion aircraft. The Harpoon was also adapted for use on USAF B-52H bombers, which can carry from 8 to 12 of the missiles. The Harpoon missile has been integrated on foreign F-16 aircraft and is presently being integrated on foreign F-15 aircraft [16]. Various variants of the missile was developed since 1977 and it was carried by more than 600 ships, 180 submarines, 12 different types of aircraft, and several land-based launch vehicles [18].

The air launched version of the missile (AGM-84A) is selected as a baseline configuration. Basic specifications of the missile are given in Table 2-1 and its configuration is shown in Figure 2-1.

**Table 2-1 AGM-84A Harpoon Missile specifications, [16] [17] [18] [19] [20]**

| | |
|---|---|
| Length | 3.85 m |
| Diameter | 0.343 m |
| Wing/Tail Span | 0.91 m |
| Launch Weight | 526 kg |
| Fuel Weight | 45 kg |
| Airframe | Cylindrical body of uniform diameter with blunt nose<br>4 wings at just aft of mid-body and in-line<br>4 control fins at the rear |
| Midcourse Guidance | Three axis integrated digital computer/strapdown attitude reference system |
| Terminal Guidance | Active Radar |
| Warhead | 222 kg high explosive blast penetration warhead |
| Propulsion | Teledyne CAE-J402 turbojet engine developing 660 lb. static thrust |
| Cruise Speed | 0.75 Mach |
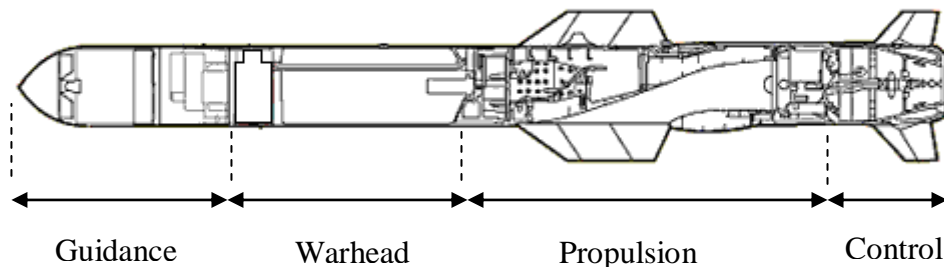


**Figure 2-1 AGM-84A Harpoon Missile configuration, [19]**

## 2.2 Missile Flight Simulation

A 6-DOF simulation of the Harpoon Missile (AGM-84A) was modeled in order to generate data for estimation process. The simulation was developed in MATLAB/Simulink environment. In this section the main blocks and signal interface between blocks are introduced.

The simulation is composed of two main sub-blocks which are AGM-84 Harpoon Missile Model block and 6DOF flight mechanic block. In addition to these main-sub-blocks standard atmosphere and gravity model blocks are also included in the model to calculate necessary atmospheric and gravitational properties. The missile model block consist of 5 sub-blocks which are Inertial Measurement Unit block, Missile Computer block, Control Actuation System block, Turbojet Engine block and Mass Properties block. In the Inertial Measurement block inertial sensors which are measuring missile translational and rotational movements are modeled. The model covers sensor bias, scale factor and noise characteristics. In the Missile Computer block 3 sub-blocks are modeled which are Inertial Navigation System, Altitude Hold System and Autopilot System. In the Control Actuation System block a second order non-linear actuator is modeled. In the turbo-jet engine block a constant thrust is modeled which satisfies a level flight for the missile. In the Mass Properties block missile mass, center of gravity and moment of inertia properties are modeled.

The 6-DOF Missile Flight Simulation architecture and main signal interfaces between simulation blocks are shown in Figure 2-2. The equations used in the simulation blocks and the detail properties of simulation blocks are presented in the remainder of this chapter.
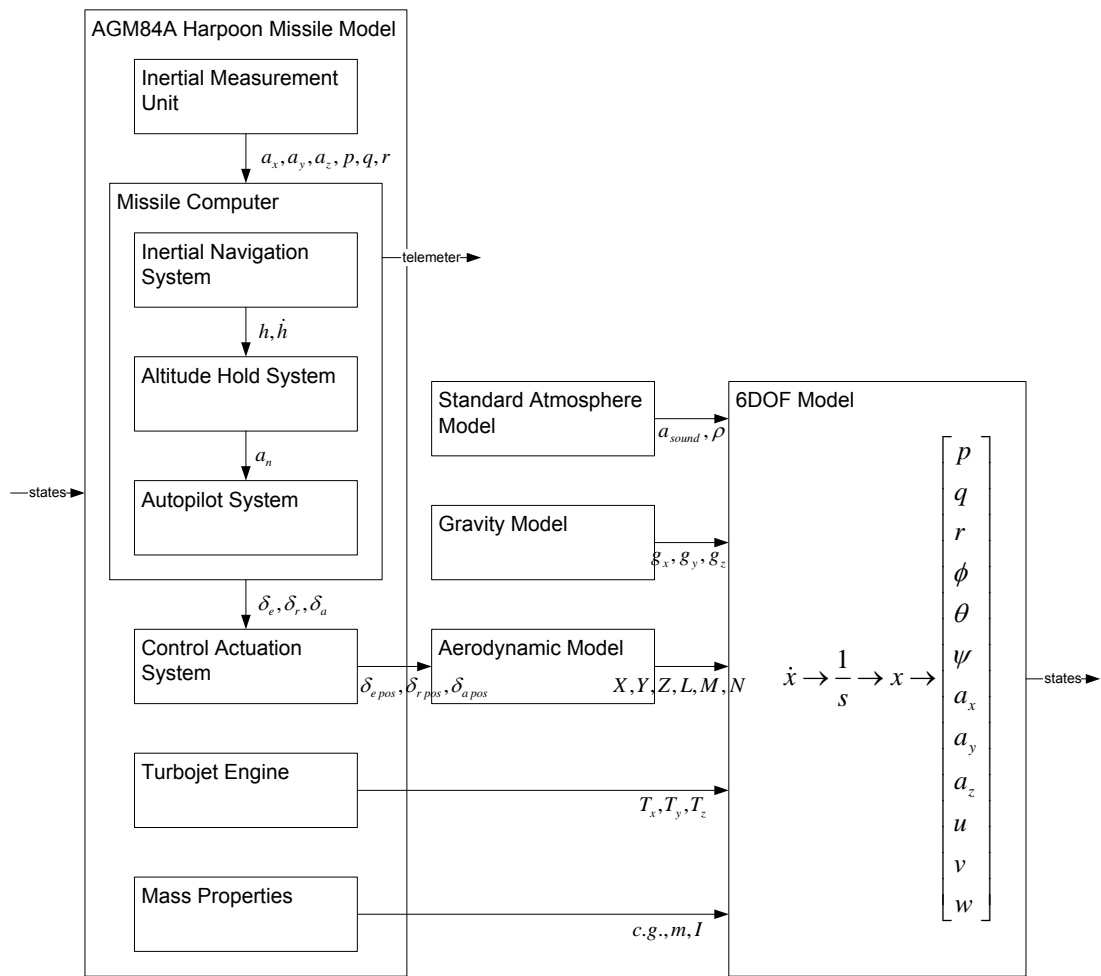
**Figure 2-2 6-DOF Missile Flight Simulation architecture**

## 2.2.1 Modeling Assumptions and Reference Frames

Before developing flight simulation the following simplifying assumptions are made.

- The earth is fixed in inertial space.

- The missile is a rigid body and symmetric in the pitch and yaw plane.

- Gravitational acceleration is constant in magnitude and direction.

- Thrust is directed along the missile body and through the center of gravity.

- Flight in earth's atmosphere is close to the earth's surface (on an astronomical scale), so the earth's surface can be approximated as flat.

In the scope of this thesis inertial axes and body axes reference frames are used. The origin of this reference frame is fixed or moving with a constant velocity to the distant stars, and the orientation is arbitrary fixed [21]. Whereas body axes reference frame has origin at the center of gravity (c.g.), with positive x axis pointing forward through the nose, positive y axis out the right wing and positive z axis trough the underside [21]. Both inertial and body axes reference frames are right handed and with mutually orthogonal axes.

Inertial and body axes reference frames are shown in Figure 2-3.
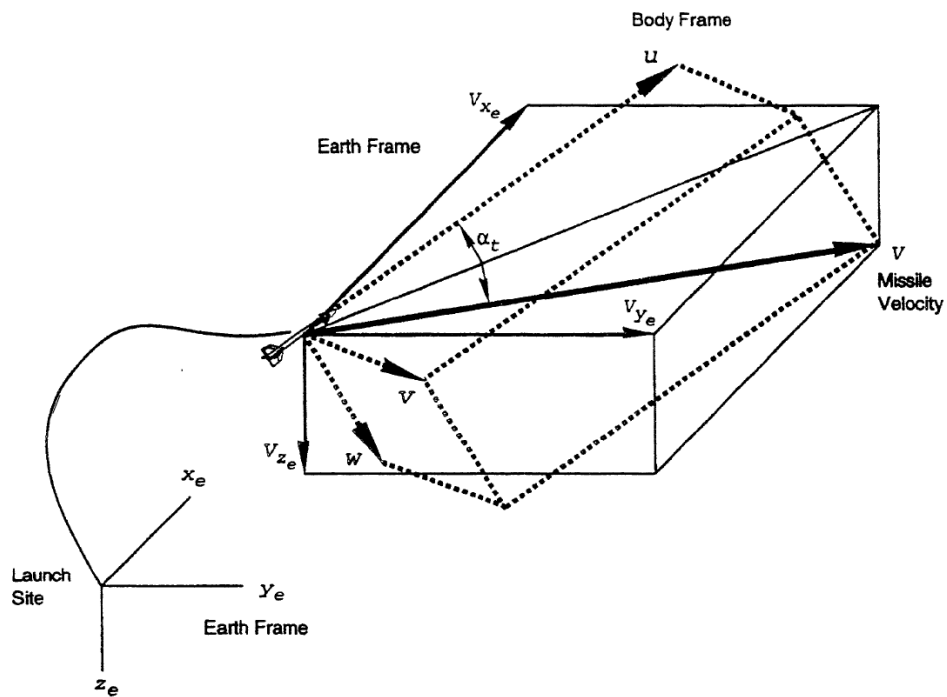


**Figure 2-3 Inertial and body axis reference frames, [21]**

## 2.2.2  Standard Atmosphere and Gravity Model

Air Density and speed of sound are calculated using Standard Atmosphere Model assuming that the missile does not fly over the altitude of 11 km [22]. The quantities Mach number and dynamic pressure are calculated using these atmospheric properties. The atmospheric properties are modeled as follows:

Temperature:

$$T = T_{SL} + a \cdot h \tag{2-1}$$

Density:

$$\rho = \rho_{SL} \cdot \left(\frac{T}{T_{SL}}\right)^{\frac{-g}{1+a \cdot R}} \tag{2-2}$$

Speed of Sound:

$$a_{sound} = \sqrt{\gamma \cdot R \cdot T} \tag{2-3}$$

where

| | | |
|---|---|---|
| $h =$ | altitude | m |
| $T =$ | temperature | K |
| $\rho =$ | density of air | kg/m$^3$ |
| $a_{sound} =$ | speed of sound | m/s |
| $T_{SL} =$ | sea level temperature | 288.16 K |
| $\rho_{SL} =$ | density of air at sea level | 1.225 kg/m$^3$ |
| $R =$ | specific gas constant | 287 J/(kgK) |
| $a =$ | lapse rate for h<11 km | -0.0065K/m |
| $g =$ | gravitational constant | 9.80665 m/s$^2$ |
| $\gamma =$ | ratio of specific heats for constant volume and constant pressure of air 1.4 | |

Gravity is assumed constant in magnitude and direction. The magnitude of gravitational acceleration is assumed as 9.80665 m/s$^2$ [23]. Its direction is always in the z direction according to the inertial reference frame defined in the section 2.2.1.

## 2.2.3 Aerodynamic Model

Aerodynamic model computes aerodynamic forces and moments according to the selected mathematical structure of the aerodynamic model. The mathematical structure is generated by simplifying assumptions considering the missile flight regime.

Based on dimensional analysis, the nondimensional aerodynamic force and moment coefficients for rigid missile can be characterized as a function of nondimensional quantities as follows [1]:

$$C_i = C_i(\alpha, \beta, \delta, \frac{\Omega l}{V}, \frac{\dot{\Omega} l^2}{V^2}, \frac{\dot{V} l}{V^2}, \frac{\omega l}{V}, \frac{\rho V l}{\mu}, \frac{V^2}{\lg}, \frac{V}{a}, \frac{m}{\rho l^3}, \frac{I}{\rho l^5}, \frac{tV}{l}) \qquad (2\text{-}4)$$

for $i = X, Y, Z, L, M, N$, where

| | | |
|---|---|---|
| $\delta =$ | control surface deflections | rad |
| $\Omega =$ | stability axis rotation rate | rad/s |
| $l =$ | characteristic length | m |
| $m =$ | mass | kg |
| $\omega =$ | oscillation frequency | rad/s |
| $t =$ | time | s |

$\dfrac{\mu}{\rho} = \nu =$      kinematic viscosity    m$^2$/s

$\dfrac{\omega l}{V} = Str =$      Strouhal Number, unsteady oscillatory flow effects

$\dfrac{\rho V l}{\mu} = \text{Re} =$      Reynolds Number, fluid inertial forces/viscous forces

$\dfrac{V^2}{gl} = Fr =$      Froude Number, inertial forces/gravitational forces

$\dfrac{V}{a_{sound}} = M =$      Mach Number, fluid compressibility effects

Common simplifications are that the missile mass and inertia significantly larger than the surrounding air mass and inertia, fluid properties change slowly, and Froude number effects are small [1]. In addition, the flow is often assumed to be quasi-steady, which means that the flow field adjusts instantaneously to changes [1]. One exception to this is the retention of Strouhal number effects, also called reduced frequency effects [1]. These assumptions reduce the preceding relationship to

$$C_i = C_i(\alpha, \beta, \delta, \frac{\Omega l}{V}, \frac{\omega l}{V}, \frac{\rho V l}{\mu}, \frac{V}{a})$$
(2-5)

Reynolds Number effects can be neglected since it changes only slightly in flight. The effects of rotary motion and forced oscillation are usually modeled as a function of the body axis angular rates, air incidence angles and their first-time derivative [1]. So equation 2-5 becomes

$$C_i = C_i(\alpha, \beta, \delta, \frac{pl}{2V}, \frac{ql}{2V}, \frac{rl}{2V}, \frac{\dot{\alpha} l}{2V}, \frac{\dot{\beta} l}{2V}, \frac{V}{a})$$
(2-6)

The aerodynamic model mathematical structure used in the simulation is based on equation 2-6. Further simplifications are done for Mach number and first-time derivatives of air incidence angles. Since missile flight almost constant speed, fluid compressibility effects can be neglected. In addition to that dynamic derivatives come from first-time derivatives of air incidence angles are small compare to body axis angular rates. The six aerodynamic coefficients are defined as follows after simplifications.

$$C_x = C_x(\alpha, \beta, \delta_e, \delta_r, \delta_a)$$
(2-7)

$$C_y = C_y(\beta, \delta_r, \frac{rl}{2V})$$
(2-8)

$$C_z = C_z(\alpha, \delta_e, \frac{ql}{2V})$$ (2-9)

$$C_l = C_l(\alpha, \beta, \delta_a, \frac{pl}{2V})$$ (2-10)

$$C_m = C_m(\alpha, \delta_e, \frac{ql}{2V})$$ (2-11)

$$C_n = C_n(\beta, \delta_r, \frac{rl}{2V})$$ (2-12)

The aerodynamic static and dynamic coefficients are calculated using U.S. Air Force DATCOM [24]. At each computation time of the flight simulation the aerodynamic coefficients interpolated using body axis angular rates and air incidence angles.

U.S. Air Force DATCOM calculates aerodynamic coefficients for given geometric properties of the missile. The basic geometric data used as the input for DATCOM are missile's section lengths, diameter, wings span and chord lengths. The geometric properties of AGM-84A Harpoon Missile are collected from open sources given in section 2.1. The unavailable physical information required for the DATCOM is calculated from Figure 2-4 assuming that it is a scaled drawing. The diameter of the missile is taken as reference or characteristic length $l$ and cross-sectional area of the missile is taken as reference area $S$ for the aerodynamic analyses.
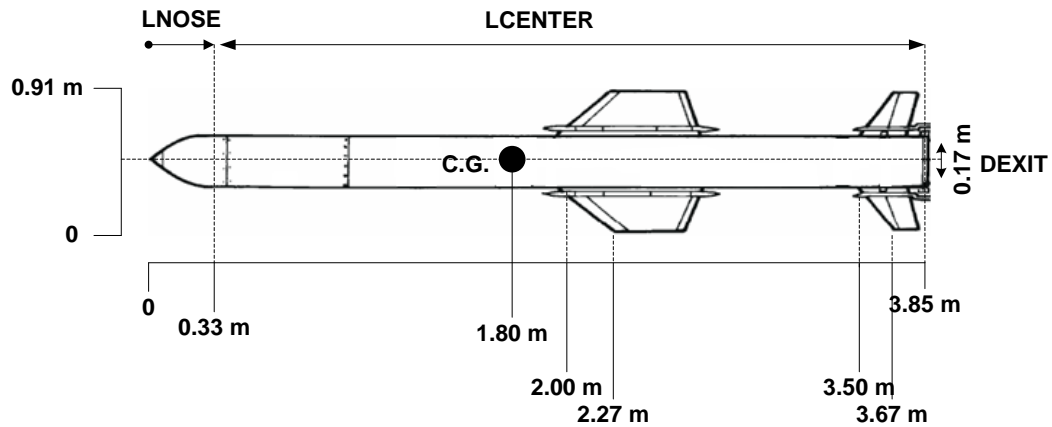
**Figure 2-4 AGM-84A Harpoon Missile dimensions**

The calculation range of aerodynamic coefficients of the missile for the range of Mach number, Angle of Attack, Sideslip Angle and Control Surface Deflection Angle are given in the next paragraph.

Mach vector: [0.3 0.5 0.7 0.8 1.0 1.1 1.2]

$\alpha$ vector: [-20 -18 -16 -14 -12 -10 -8 -6 -3 0 3 6 8 10 12 14 16 18 20] deg

$\beta$ vector: [-20 -18 -16 -14 -12 -10 -8 -6 -3 0 3 6 8 10 12 14 16 18 20] deg

$\delta_e$ vector: [-20 -18 -16 -14 -12 -10 -8 -6 -3 0 3 6 8 10 12 14 16 18 20] deg

$\delta_r$ vector: [-20 -18 -16 -14 -12 -10 -8 -6 -3 0 3 6 8 10 12 14 16 18 20] deg

$\delta_a$ vector: [-20 -18 -16 -14 -12 -10 -8 -6 -3 0 3 6 8 10 12 14 16 18 20] deg

Analyzing U.S. Air Force DATCOM's axial force coefficient $C_x$ calculation results in Figure 2-5 it can be seen that $C_x$ numbers increases dramatically above Mach number 0.8 so that the cruise speed of the missile is selected as Mach number 0.75. The $C_x$ calculation results versus Mach number are shown in Figure 2-5. Since aerodynamic database is symmetric for positive and negative angle of attacks, only $C_x$ numbers for positive angle of attack are shown for simplicity.

17
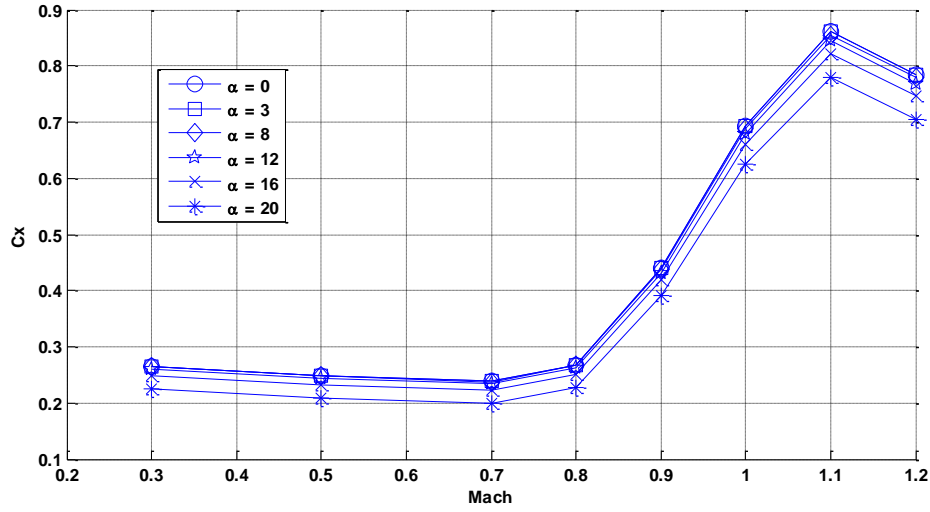
**Figure 2-5** $C_x$ **versus Mach number**

Further investigation of aerodynamic database of the AGM-84A Harpoon Missile is done for autopilot design in section 2.2.5.1.

### 2.2.4   6-DOF Model

In the 6-DOF Model block force and moment are summed to calculate missile states in the next computation time. At his block the following equations of motion are used [1, 21].

Force equations:

$$\dot{u} = rv - qw + \frac{QS}{m}C_x - g\sin\theta + \frac{T}{m} \tag{2-13}$$

$$\dot{v} = pw - ru + \frac{QS}{m}C_y - g\cos\theta\sin\phi \tag{2-14}$$

$$\dot{w} = qu - pv + \frac{QS}{m}C_z + g\cos\theta\cos\phi \tag{2-15}$$

18

Moment equations:

$$\dot{p} - \frac{I_{xz}}{I_x}\dot{r} = \frac{QSl}{I_x}C_l - \frac{(I_z - I_y)}{I_x}qr + \frac{I_{xz}}{I_x}qp \qquad (2\text{-}16)$$

$$\dot{q} = \frac{QSl}{I_y}C_m - \frac{(I_x - I_z)}{I_y}pr - \frac{I_{xz}}{I_y}(p^2 - r^2) \qquad (2\text{-}17)$$

$$\dot{r} - \frac{I_{xz}}{I_z}\dot{p} = \frac{QSl}{I_z}C_n - \frac{(I_y - I_x)}{I_z}pq - \frac{I_{xz}}{I_z}qr \qquad (2\text{-}18)$$

Rotational kinematic equations:

$$\dot{\phi} = p + \tan\theta(q\sin\phi + r\cos\phi) \qquad (2\text{-}19)$$

$$\dot{\theta} = q\cos\phi - r\sin\phi \qquad (2\text{-}20)$$

$$\dot{\psi} = \frac{q\sin\phi + r\cos\phi}{\cos\theta} \qquad (2\text{-}21)$$

Total velocity, angle of attack, sideslip angle:

$$V_T = \sqrt{u^2 + v^2 + w^2} \qquad (2\text{-}22)$$

$$\alpha = \tan^{-1}(\frac{w}{u}) \qquad (2\text{-}23)$$

$$\beta = \tan^{-1}(\frac{v}{V_T}) \qquad (2\text{-}24)$$

The position of the missile is calculated from the integration of the missile velocity which is transformed to the inertial reference frame given in the section 2.2.1. The transformation matrix $L_{EB}$ is given below [1, 21].

$$L_{EB} = \begin{bmatrix} \cos\theta\cos\psi & \sin\phi\sin\theta\cos\psi - \cos\phi\sin\psi & \cos\phi\sin\theta\cos\psi + \sin\theta\sin\psi \\ \cos\theta\sin\psi & \sin\phi\sin\theta\sin\psi + \cos\phi\cos\psi & \cos\phi\sin\theta\sin\psi - \sin\phi\cos\psi \\ -\sin\theta & \sin\phi\cos\theta & \cos\phi\cos\theta \end{bmatrix} \quad (2\text{-}25)$$

## 2.2.5 AGM-84A Harpoon Missile Model

AGM-84A Missile Model consists of 5 main blocks which are Missile Computer, Inertial Measurement Unit, Control Actuation System, Turbojet Engine and Mass Properties. In this section of this work the details of calculations done at each block are given.

### 2.2.5.1 Missile Computer

Missile Computer consists of three sub-blocks which are Inertial Navigation System, Autopilot System and Altitude Hold System. These three sub-blocks can be considered serial calculation of tail position command in the next computation time of the simulation.

#### 2.2.5.1.1 Inertial Navigation System

Inertial Navigation System simply calculates translational and rotational states of the missile using translational acceleration and rotational velocity measured by Inertial Measurement Unit. The output of this block is used by Altitude Hold System and Autopilot System sub-blocks. The block diagram of the Inertial Navigation System is in Figure 2-6.
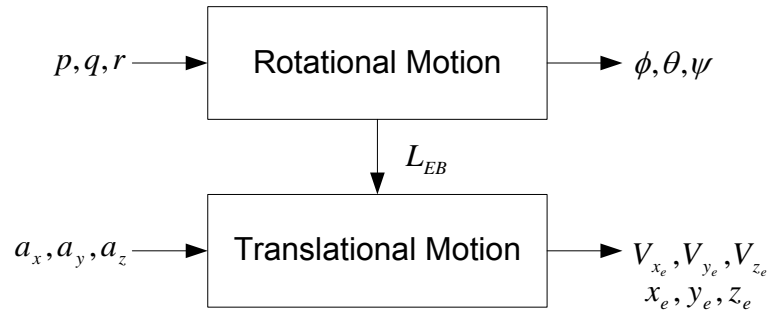
**Figure 2-6 Inertial Navigation System block diagram**

The block calculates rotational and translational motion of the missile. The rotational motion of the missile is calculated directly using Inertial Measurement Unit outputs. At each computation time the Euler angles of the missile are calculated using Equations 2-19, 2-20 and 2-21. The calculated Euler angles are also used for generating transformation matrix $L_{EB}$ which is given in Equation 2-25. Missile inertial coordinates, inertial velocity, Mach number, air incidence angles are calculated by using Inertial Measurement Unit axial acceleration and transformation matrix. The outputs of this block are sent to the Autopilot System and Altitude Hold System blocks.

### 2.2.5.1.2 Autopilot System

A linear acceleration autopilot for the pitch and yaw channel and a linear angle autopilot for the roll channel are used in the flight simulation. In this work the estimation of longitudinal aerodynamic parameters is focused. So that design of the longitudinal autopilot is given in detail in the remainder of this section.

Modeled acceleration autopilot for the longitudinal channel calculates required tail position commands for desired acceleration command. A state feedback controlled autopilot is designed for the simulation. Since all the states are measured roots can be placed in the desired locations in order to satisfy performance characteristics. As the missile is symmetric in the pitch and yaw plane only one autopilot is designed for

both axes. The block diagram of the Autopilot System is shown in Figure 2-7. Remember that for yaw autopilot the states $\alpha, q, \delta_e$ and $\dot{\delta}_e$ changes as $\beta, r, \delta_r$ and $\dot{\delta}_r$ respectively.
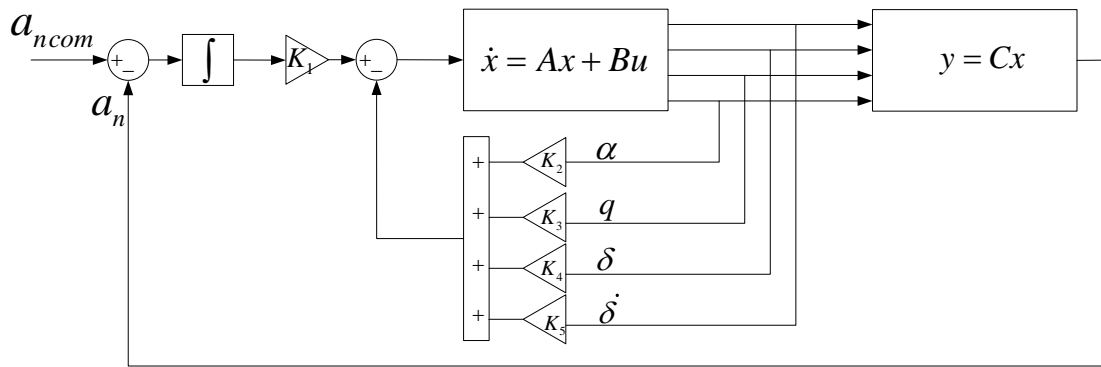


**Figure 2-7 Autopilot System block diagram**

The linear acceleration autopilot is designed using pole placement technique. The state-space matrices of the missile are as follows;

$$\dot{x} = Ax + Bu \tag{2-26}$$

$$y = Cx + Du \tag{2-27}$$

The matrices A, B, C and D in the above equations are obtained assuming that the missile flights in regime where aerodynamic forces and moments are linear. So that a linear region must be defined in aerodynamic database in order to design autopilot. Using aerodynamic curves one can obtain linear region of the system. For Mach number 0.8, normal force $C_N$ and pitch moment $C_m$ calculation of the AGM-84A Harpoon missile are given in, Figure 2-8, Figure 2-9, Figure 2-10 and Figure 2-11 with highlighted linear regions. Remember that normal force direction is negative (upward) according to body coordinate system given in section 2.2.1. Since missile is symmetric in the pitch and yaw plane the calculated normal force and pitch moment

22

coefficients can be directly used as side force $C_y$ and yaw moment $C_n$ coefficients considering positive directions.
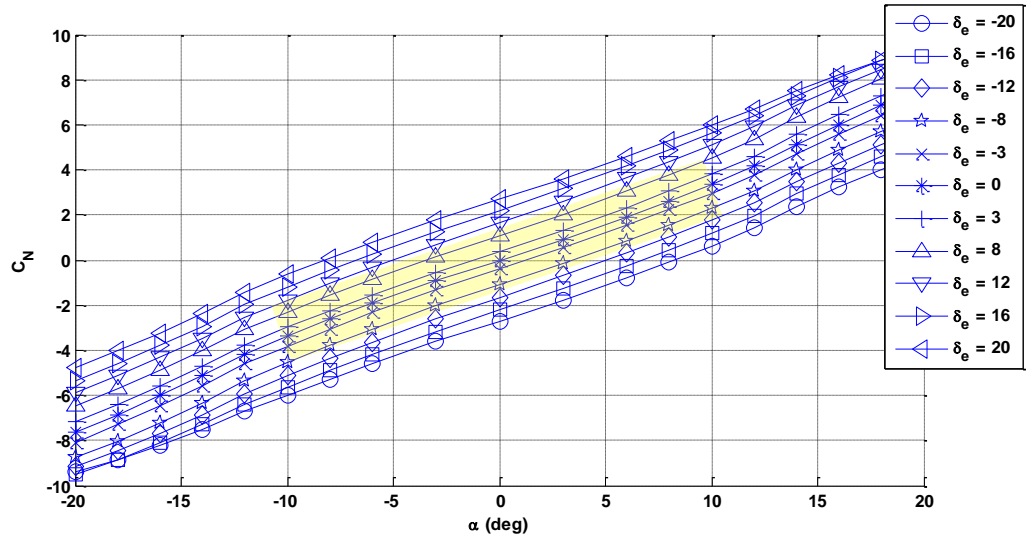


**Figure 2-8** $C_N$ **versus** $\alpha$
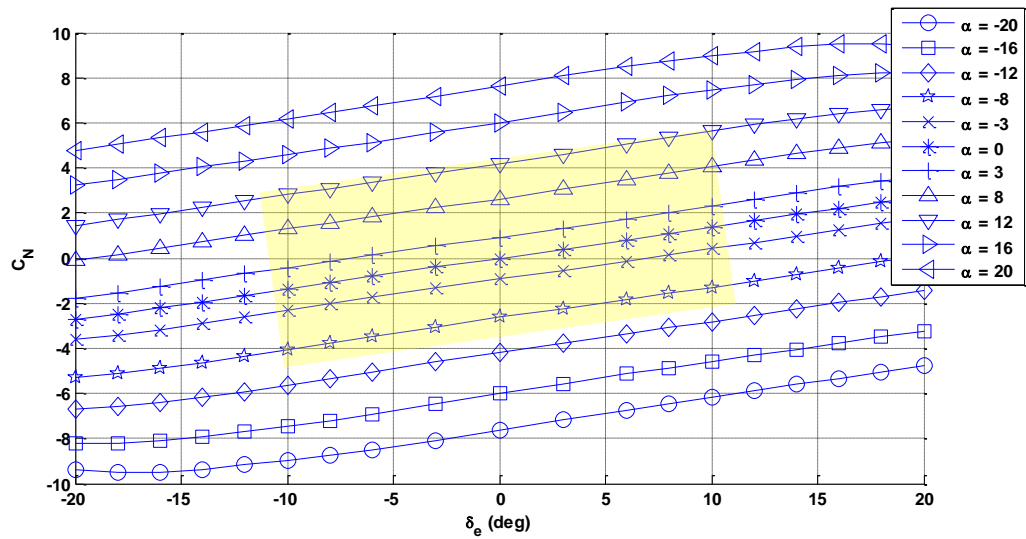


**Figure 2-9** $C_N$ **versus** $\delta_e$

23

Analyzing Figure 2-8 and Figure 2-9, the aerodynamic linear region for $C_N$ occurs in the highlighted area which covers a $\pm 10°$ angle of attack and control surface deflection region. Similar analysis for $C_m$ curves are given in the below figures.
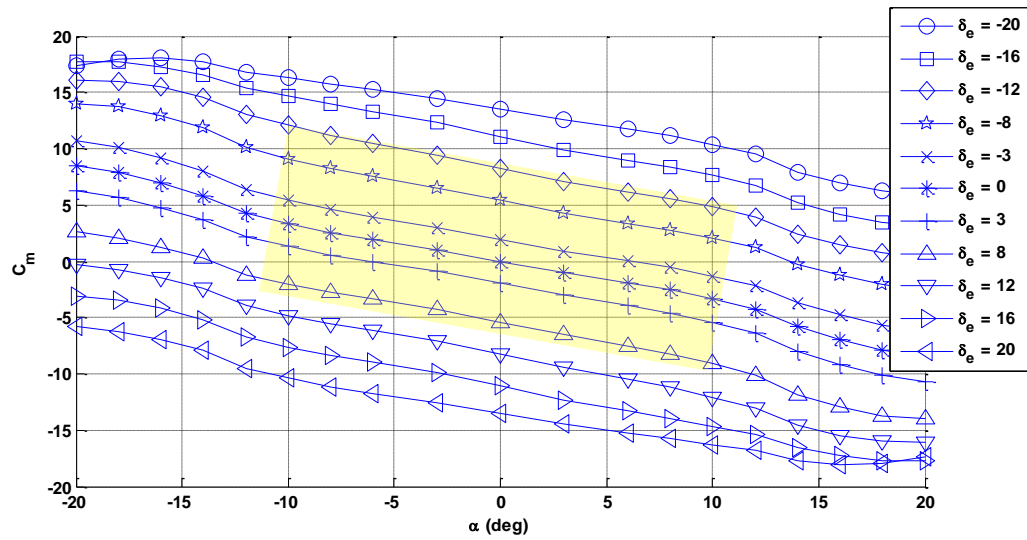


**Figure 2-10** $C_m$ **versus** $\alpha$
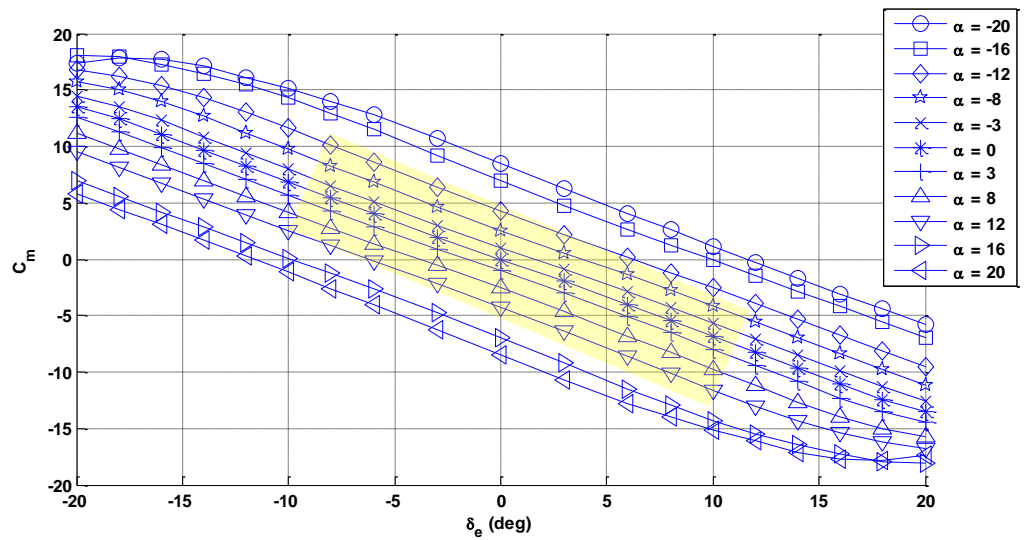


**Figure 2-11** $C_m$ **versus** $\delta_e$

Analyzing Figure 2-10 and Figure 2-11 the linear region for $C_m$ curves is very similar as $C_N$ curves. As seen from highlighted areas, the linear regions for $C_m$ curves occur again at a ±10° angle of attack and control surface deflection.

In these linear regions analyzed above one can easily calculate stability derivatives $C_{N\alpha}$, $C_{N\delta}$, $C_{m\alpha}$ and $C_{m\delta}$ using the slope of the curves. The stability derivatives calculated for Mach numbers 0.5, 0.7 and 0.8 are given in Table 2-2. The stability derivatives $C_{N\alpha}$ and $C_{m\alpha}$ are calculated above 0° control deflection curve between 0°,±10° angle of attack. Similarly $C_{N\delta}$ and $C_{m\delta}$ stability derivatives are calculated above 0° angle of attack curve between 0°, ±10° control surface deflection. The stability derivatives $C_{Nq}$ and $C_{mq}$ are obtained from U.S. Air Force DATCOM. Note that these longitudinal stability derivatives can be used as lateral stability derivatives $C_{y_r}$ and $C_{n_r}$ since missile has symmetric shape.

**Table 2-2 Aerodynamic stability derivatives**

|  | Mach; 0.5 | Mach; 0.7 | Mach; 0.8 |
|---|---|---|---|
| $C_{N\alpha}$ (1/rad) | 18.24 | 18.24 | 18.40 |
| $C_{N\delta}$ (1/rad) | 7.01 | 7.36 | 7.80 |
| $C_{m\alpha}$ (1/rad) | -17.42 | -18.24 | -19.01 |
| $C_{m\delta}$ (1/rad) | -35.08 | -36.81 | -39.02 |
| $C_{Nq}$ (1/rad) | 108.25 | 111.37 | 115.78 |
| $C_{mq}$ (1/rad) | -402.02 | -426.35 | -453.32 |

The states of the longitudinal autopilot are given by;

$$x = \begin{bmatrix} \alpha & q & \delta_e & \dot{\delta}_e \end{bmatrix} \qquad (2\text{-}28)$$

In the above equation $\delta_e$ and $\dot{\delta}_e$ represent the effect of the Control Actuation System to the system. The model used in Control Actuation System is introduced in Section 2.2.5.3. The mass properties used in the following equations are summarized in Section 2.2.5.5. The motion in the longitudinal plane can be expressed as follows;

$$F_z = mg\cos(\theta)\cos(\phi) = m(\dot{w} - qu + pv) \tag{2-29}$$

$$M = I_y\dot{q} + rp(I_x - I_z) + I_{xz}(p^2 - r^2) \tag{2-30}$$

The following assumption can be made to define linear equations from above non-linear equations.

- Roll axis motion is faster than the motion at longitudinal axis, so that $p \cong 0$.
- The effect of gravity is less than aerodynamic force in z axis, so that $mg\cos(\theta)\cos(\phi) \cong 0$.
- The missile is a rigid body and symmetric in the pitch and yaw plane, so that $I_{xz} \cong 0$.

Applying the above assumptions and rearranging Equations 2-29 and 2-30;

$$\dot{w} = \frac{F_z}{m} + qu \tag{2-31}$$

$$\dot{q} = \frac{M}{I_y} \tag{2-32}$$

Using small angle and short period approximations;

$$\alpha = \tan^{-1}(\frac{w}{u}) \tag{2-33}$$

$$\alpha \cong \frac{w}{u} \qquad (2\text{-}34)$$

$$\dot{\alpha} \cong \frac{\dot{w}}{u} \qquad (2\text{-}35)$$

Then Equation 2-31 becomes;

$$\dot{\alpha} = \frac{F_z}{mu} + q \qquad (2\text{-}36)$$

The aerodynamic force in Equation 2-36 and aerodynamic moment in 2-32 can be expressed as follows;

$$F_z = QSC_{z_\alpha}\alpha + QSC_{z_\delta}\delta + QSC_{z_q}\frac{l}{2V}q \qquad (2\text{-}37)$$

$$M = QSlC_{m_\alpha}\alpha + QSlC_{m_\delta}\delta + QSlC_{m_q}\frac{l}{2V}q \qquad (2\text{-}38)$$

Combining Equations 2-32, 2-36 with 2-37 and 2-38 the following equations are obtained.

$$\dot{\alpha} = q + Z_\alpha\alpha + Z_\delta\delta + Z_q q \qquad (2\text{-}39)$$

$$\dot{q} = M_\alpha\alpha + M_\delta\delta + M_q q \qquad (2\text{-}40)$$

where

$$Z_\alpha = \frac{QS}{mV}C_{z_\alpha} \qquad (2\text{-}41)$$

$$Z_\delta = \frac{QS}{mV}C_{z_\delta} \qquad (2\text{-}42)$$

$$Z_q = \frac{QS}{mV} \frac{l}{2V} C_{z_q} \tag{2-43}$$

$$M_\alpha = \frac{QS}{I_y} l C_{m_\alpha} \tag{2-44}$$

$$M_\delta = \frac{QS}{I_y} l C_{m_\delta} \tag{2-45}$$

$$M_q = \frac{QS}{I_y} \frac{l}{2V} l C_{m_q} \tag{2-46}$$

Combining Control Actuation System model and using Equation 2-39 with 2-40 the state space representation of the missile longitudinal motion expressed as follows;

$$\begin{bmatrix} \dot{\alpha} \\ \dot{q} \\ \dot{\delta}_e \\ \ddot{\delta}_e \end{bmatrix} = \begin{bmatrix} Z_\alpha & 1+Z_q & Z_\delta & 0 \\ M_\alpha & M_q & M_\delta & 0 \\ 0 & 0 & 0 & 1 \\ 0 & 0 & -w_n^2 & -2\zeta w_n \end{bmatrix} \cdot \begin{bmatrix} \alpha \\ q \\ \delta_e \\ \dot{\delta}_e \end{bmatrix} + \begin{bmatrix} 0 \\ 0 \\ 0 \\ w_n^2 \end{bmatrix} \cdot u \tag{2-47}$$

Remember that the aim is designing a linear acceleration autopilot in the longitudinal plane, than the measurement is the normal force defined by the following formula;

$$a_n = F_z / m \tag{2-48}$$

Combining Equation 2-37 with 2-48 the measurement matrix is obtained as follows;

$$a_n = \begin{bmatrix} \frac{QS}{m} C_{z_\alpha} & \frac{QS}{m} \frac{l}{2V} C_{z_q} & \frac{QS}{m} C_{z_\delta} & 0 \end{bmatrix} \cdot \begin{bmatrix} \alpha \\ q \\ \delta_e \\ \dot{\delta}_e \end{bmatrix} \tag{2-49}$$

For Mach number 0.8 the eigenvalues i.e. the roots of the characteristic equation of the system matrix $A$ is;

**Table 2-3 Open Loop eigenvalues**

| |
|---|
| -0.6048 + 6.6152i |
| -0.6048 - 6.6152i |
| -87.9646 +89.7418i |
| -87.9646 -89.7418i |

Since all the values have negative sign, the open loop transfer function from $\delta_e$ to $a_n$ is stable. The frequency response characteristic of the open loop system gives important information about the system. The frequency response characteristic of transfer function from control surface input to normal acceleration for Mach number 0.8 is given in Figure 2-12. As shown from figure the maximum peak response of the system is occurred at 1.05 Hz. This frequency is the airframe natural frequency and can be also calculated from;

$$w_n = \sqrt{-M_\alpha} \qquad (2\text{-}50)$$

Choosing an excitation signal contain wide frequency spectrum including airframe natural frequency is critical point to sustain enough information in order to get good estimation results which is widely discussed in section 3.3.1. The airframe natural frequencies for Mach numbers 0.5, 0.7 and 0.8 are given in Table 2-4.

**Table 2-4 AGM-84A Harpoon Missile airframe natural frequencies**

| | Mach; 0.5 | Mach; 0.7 | Mach; 0.8 |
|---|---|---|---|
| $w_n$ (Hz) | 0.6301 | 0.9027 | 1.053 |
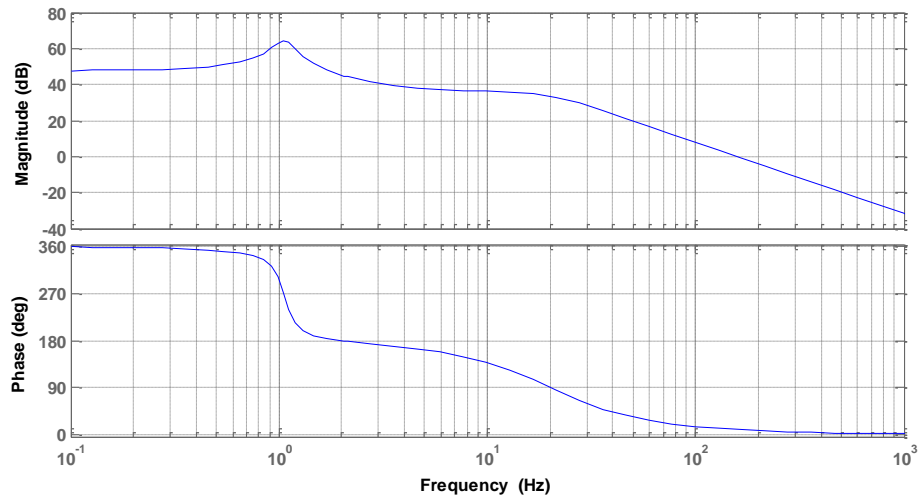
**Figure 2-12 Open Loop System frequency response**

In the longitudinal autopilot design process poles are placed so that desired transient performance characteristics are achieved. The desired performance characteristics are defined by the dominant poles of the system. Since there is integrator in closed loop system to compensate steady-state error, five poles must be placed in desired locations. The poles vector is shown in Equation 2-51.

$$P = \begin{bmatrix} -a+bi & -a-bi & -c & -d+ei & -d-ei \end{bmatrix} \qquad (2\text{-}51)$$

Considering open loop poles, poles coming from Control Actuation System is far away from the poles of the airframe. The fast poles of Control Actuation System are held as it is. Placing the remaining three poles at desired locations one can calculate state feedback gain matrix. Choosing the real pole "c" constant, the effect of the real part of the remaining poles are examined. The gain matrix for every controller is calculated by using MATLAB's "place" command. The selected poles are summarized in Table 2-5.

**Table 2-5 Longitudinal autopilot desired poles**

|  | Controller 1 | Controller 2 | Controller 3 | Controller 4 |
|---|---|---|---|---|
| P1 | -5+5i | -10+5i | -15+5i | -20+5i |
| P2 | -5-5i | -10-5i | -15-5i | -20-5i |
| P3 | -10 | -10 | -10 | -10 |
| P4 | -87.9+89.7i | -87.9+89.7i | -87.9+89.7i | -87.9+89.7i |
| P5 | -87.9-89.7i | -87.9-89.7i | -87.9-89.7i | -87.9-89.7i |

For every controller transient performance characteristics to a step command are calculated. The results are given in Figure 2-13 and Table 2-6. Note that as the real part magnitude of the poles P1 and P2 increases closed loop system becomes faster. On the contrary the percent undershoot of the system increases which is not desired.
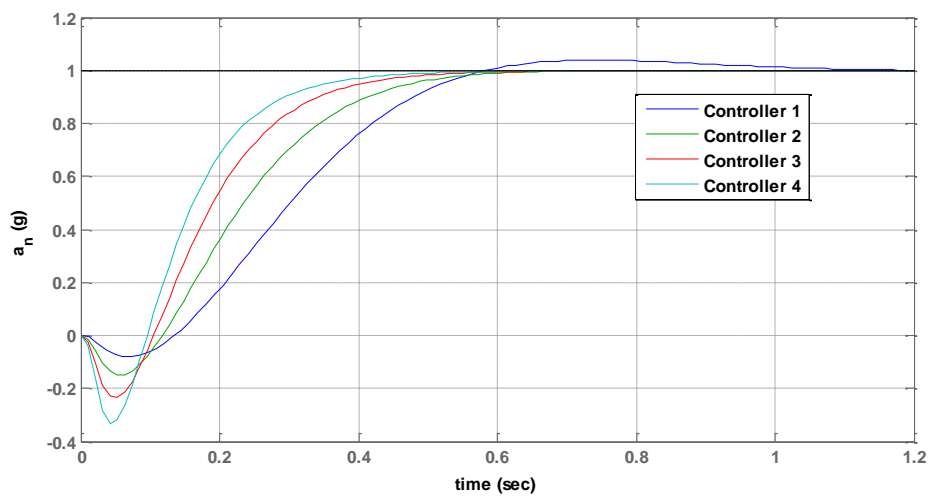


**Figure 2-13 Step Response comparison of controllers**

**Table 2-6 Longitudinal autopilot transient performance characteristics**

|  | Controller 1 | Controller 2 | Controller 3 | Controller 4 |
|---|---|---|---|---|
| Rise Time (s) | 0.31 | 0.27 | 0.22 | 0.19 |
| Settling Time (s) | 0.92 | 0.54 | 0.47 | 0.41 |
| Overshoot (%) | 3.86 | 0.02 | 0 | 0 |
| Undershoot (%) | 8.04 | 14.92 | 23.59 | 33.17 |

The frequency response characteristics of the closed loop system for designed controllers are also examined. As seen from Figure 2-14, bandwidth of the closed loop system increases with the increasing magnitude of the real part of the poles P1 and P2.
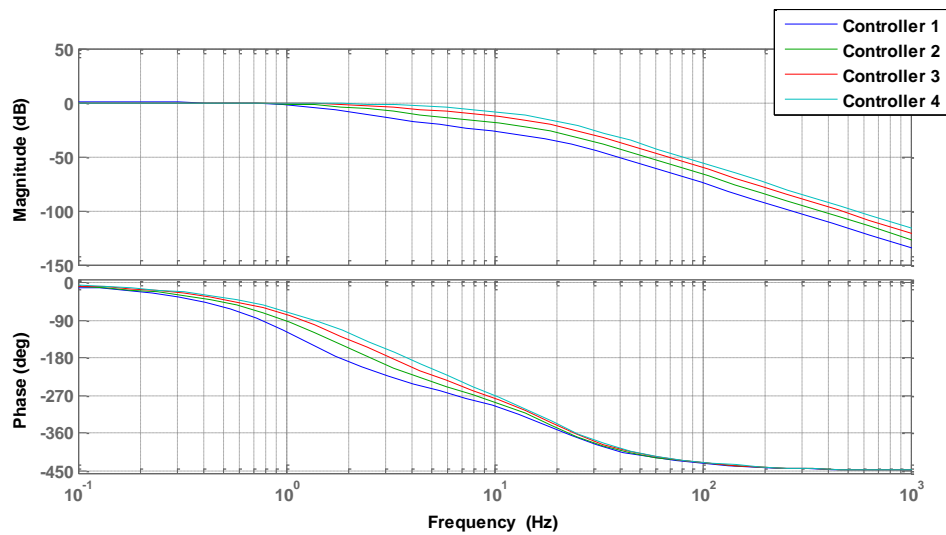


**Figure 2-14 Frequency Response comparison of controllers**

Until this part of this section transient performance and frequency response are examined for different controllers. Remember that the focus of this work is aerodynamic parameter estimation from closed loop data which is done by excitation system with separate surface excitations. The focus of this thesis brings forward of examination of disturbance rejection characteristics of the autopilot.

The separate surface excitations treated as disturbance by the autopilot and they are applied to the system via adding autopilot commands. The block diagram of the application of separate surface excitations is shown in Figure 2-15.
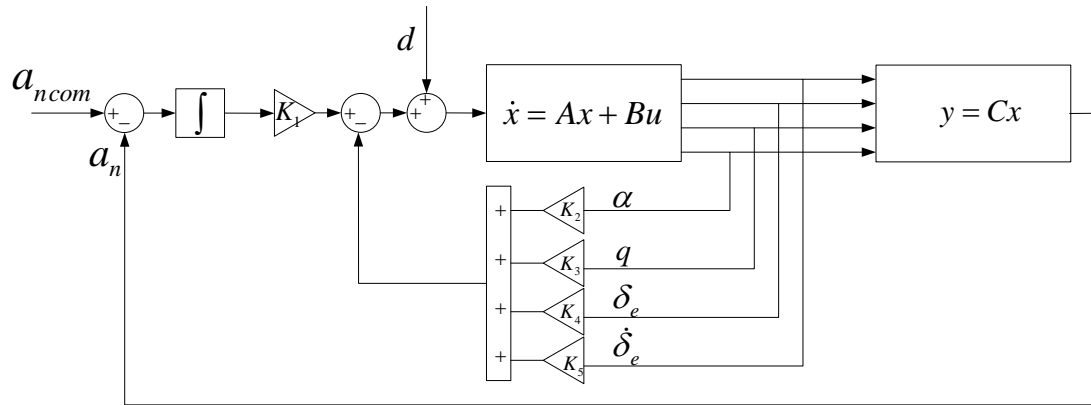


**Figure 2-15 Autopilot System block diagram with input disturbance**

The input disturbance rejection characteristics of the autopilot can be studied by examining the transfer function from input disturbance to the output. The following transfer functions are obtained for designed controllers;

Controller 1;

$$\frac{y(s)}{d(s)} = -7.958e - 13\frac{s^3(s+1.261e18)}{(s+5-5i)(s+5+5i)(s+10)(s+87-89.7418i)(s+87-89.7418i)}$$

Controller 2;

$$\frac{y(s)}{d(s)} = -7.389e - 13\frac{s^3(s+1.358e18)}{(s+15-5i)(s+15+5i)(s+10)(s+87-89.7418i)(s+87-89.7418i)}$$

Controller 3;

$$\frac{y(s)}{d(s)} = 1.421e - 13\frac{s^3(s-7.064e18)}{(s+15-5i)(s+15+5i)(s+10)(s+87-89.7418i)(s+87-89.7418i)}$$

Controller 4;

$$\frac{y(s)}{d(s)} = -6.821e - 13 \frac{s^3(s+1.471e18)}{(s+20-5i)(s+20+5i)(s+10)(s+87-89.7418i)(s+87-89.7418i)}$$

As seen from transfer functions all transfer functions are stable. The roots of the transfer functions are same with the roots of the designed Autopilot System for each controller. It can be concluded that Autopilot System will reject the input disturbance in its designed region since transfer functions from $d$ to $y$ are stable. In other words stability is conserved in the designed region of the Autopilot System for given input disturbances. Step response of transfer functions from input disturbance $d$ to output $y$ is also examined. As seen from the Figure 2-16 each designed controller rejects step input disturbance which has frequency spectrum within the bandwidths of the controllers. In addition to that as bandwidth of the controller increases its disturbance rejection performance also increases.
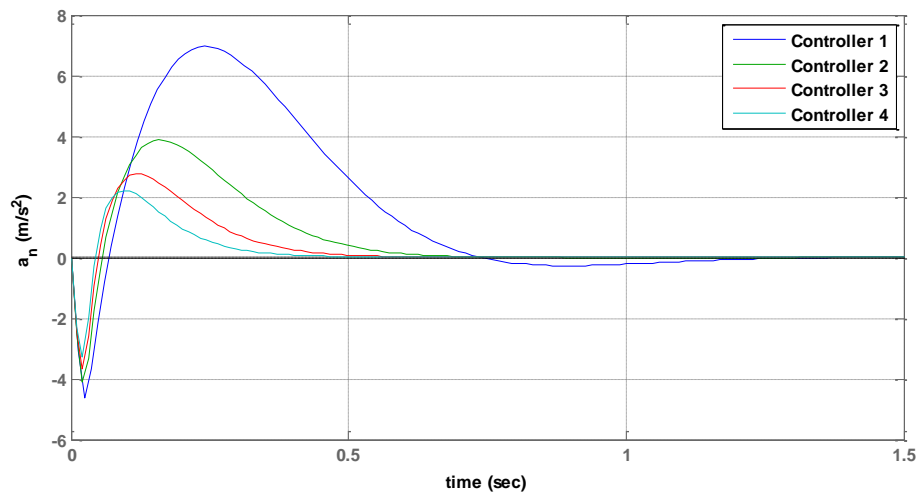


**Figure 2-16 Step Disturbance response comparison of controllers**

The disturbance rejection characteristics of autopilot can be seen more detailed in frequency response analysis. The frequency response analysis of input disturbance

rejection for designed autopilots is given Figure 2-17. Note that the open loop frequency response is also added to this figure for detailed discussion. As seen from Figure 2-17 the magnitude of output to input decreases as closed loop system bandwidth increases. In other words input disturbance rejection capability of the feedback control increases with increasing bandwidth. In addition to that above bandwidth frequencies of the closed loop system, closed loop system acts like open loop system since it cannot react those frequencies.
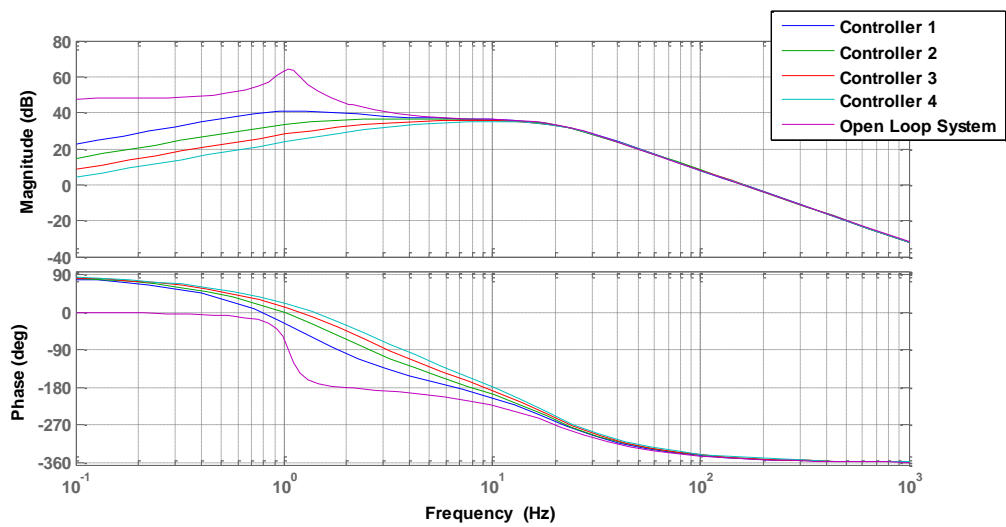


**Figure 2-17 Input disturbance frequency response comparison of controllers**

As stated preceding paragraphs input disturbance rejection performance is directly related to the focus of this work which is aerodynamic parameter estimation from closed loop data. As feedback controller rejection capacity increases to input disturbances, it is harder to collect necessary information for estimation process. In other words the open loop response of the system is shadowed by the feedback controller. This subject is studied more detailed in Section 3.3.1.

For further analyses a controller is selected from designed alternatives. Keeping percent undershoot under % 20, Controller-2 is selected for Mach number 0.8.

Keeping similar transient performance characteristics poles are selected for Mach numbers 0.5 and 0.7. The calculated state feedback controller gains are given below.

**Table 2-7 State feedback controller gains**

|  | Mach; 0.5 | Mach; 0.7 | Mach; 0.8 |
|---|---|---|---|
| K1 | -3.2932 | -3.1119 | -2.9104 |
| K2 | -0.4733 | -0.4514 | -0.4249 |
| K3 | 0.3376 | 0.3370 | 0.3363 |
| K4 | 0.0018 | 0.0018 | 0.0018 |
| KI | -0.1285 | -0.1239 | -0.1167 |

### 2.2.5.1.3 Altitude Hold System

Altitude Hold System calculates necessary guidance command in order maintain level flight of the missile. In other words missile can fly at desired altitude. The block diagram of the Altitude Hold System used in the simulation is shown in the Figure 2-18 .
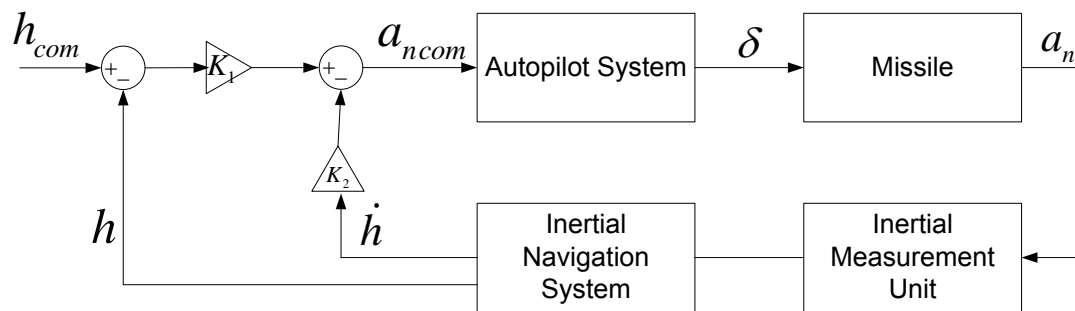


**Figure 2-18 Altitude Hold System block diagram**

All the following estimation analyses shown in Section 3 are made while missile is flight in a trimmed level flight condition. Therefore following assumptions are made before designing K1 and K2 gains for the altitude hold system.

-       $\theta$ and $\alpha$ are small enough so that $\dot{h} = V_z \cong \int a_z$ and $h \cong \iint a_z$ .

Proportional gains of Altitude Hold System calculated by using transfer function generated from block diagram given in Figure 2-19, which is reduced from block diagram given in Figure 2-18 using above assumption.
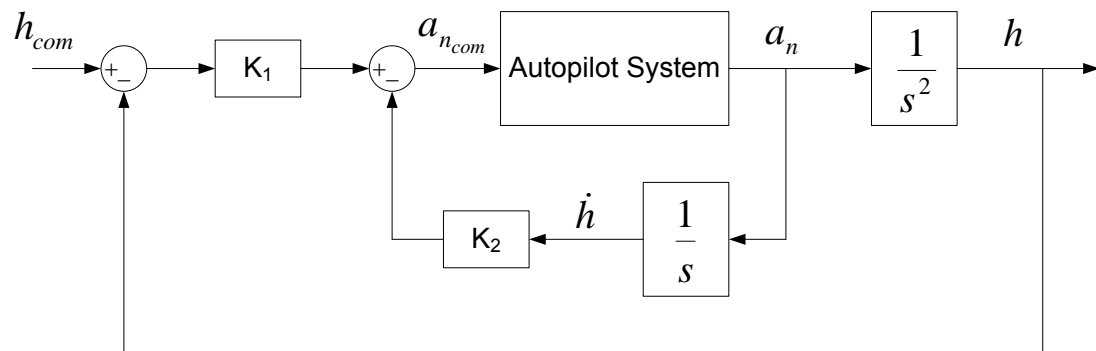


**Figure 2-19 Altitude Hold System block diagram (reduced)**

Proportional gains summarized in Table 2-9 are selected for satisfying following design criteria.

-       Maximum percent overshoot will be below 5 %

-       Rise time will be below 2 s

For Mach number 0.8, K1 is selected as 1 and K2 is selected as 1.5. The transient response characteristics of Altitude Hold System are summarized in Table 2-8.

**Table 2-8 Altitude Hold System transient performance characteristics**

|                    | Mach; 0.8 K1;1 K2; 1.5 |
| ------------------ | ---------------------- |
| Rise Time (s)      | 1.99                   |
| Settling Time (s)  | 4.68                   |
| Overshoot (%)      | 2.19                   |
| Undershoot (%)     | 0                      |

Note that maximum percent overshoot is about 2% while rise time about 2 s. The step response of Altitude Hold System for Mach number 0.8 is showed in Figure 2-20.
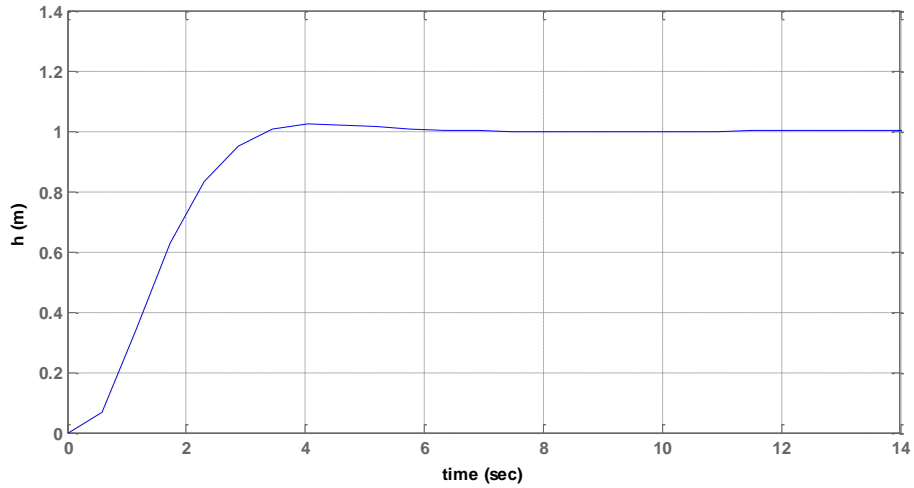


**Figure 2-20 Altitude Hold System step response**

Frequncy response of Altitude Hold System is also studied. Frequency response of Altitude Hold System for Mach number 0.8 is given in Figure 2-21.
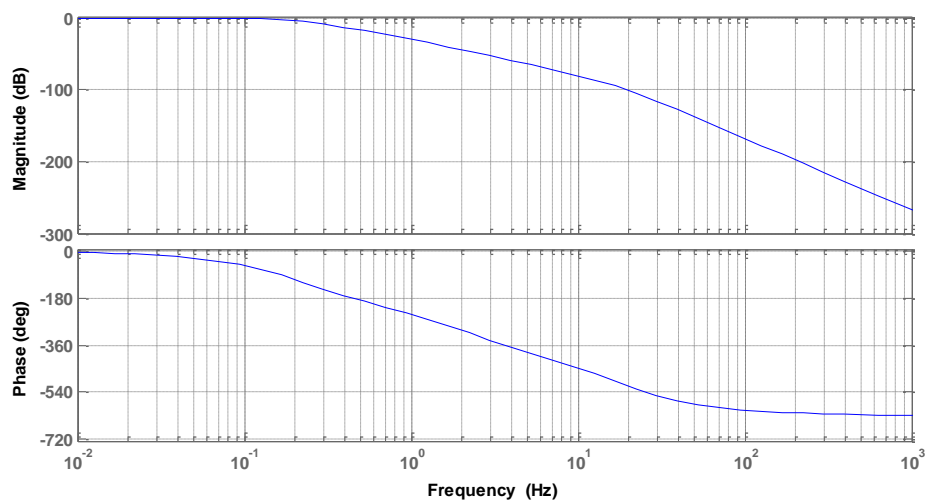


**Figure 2-21 Altitude Hold System frequency response**

As comparing Autopilot System, Altitude Hold System has smaller bandwidth. This situation can be expressed as that Altitude Hold System will give additonal rejection capacity to the Autopilot system for low frequencies. In addtion to frequency response analysis disturbance rejection performance of Altitude Hold System is examined. Disturbance rejection performance is obtained by studying transfer function from input disturbance $d$ to output $y$ shown in the block diagram given in Figure 2-22.
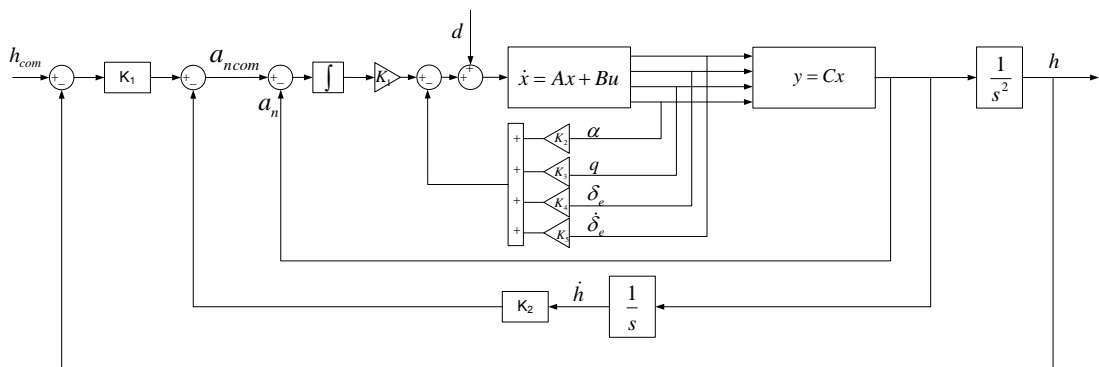


**Figure 2-22 Altitude Hold System block diagram with input disturbance**

The following transfer function is obtianed from from input disturbance $d$ to output $y$ for Mach number 0.8.

Altitude Hold System;

$$\frac{y(s)}{d(s)} = -1e6 \frac{s^3(s-13.095)(s+12.914)}{(s+1.1-0.9i)(s+1.1+0.9i)(s+4)(s+12.1-2.9i)(s+12.1-2.9i)(s+87.4-89.7i)(s+87.4-89.7i)}$$

As seen from transfer function 3 more poles comes to the denominator comparing the transfer functions in Autopilot System. In addtion to that all poles in the denominator are in the left half plane which means that the transfer function is stable. More discussion can be made by analysing frequency response of two transfer functions from input disturbance to output which are obtained for Altitude Hold System and

for Autopilot System (i.e. Controller 2). The comparison of frequency response of Altittude Hold System and Autopilot System is given in Figure 2-23.
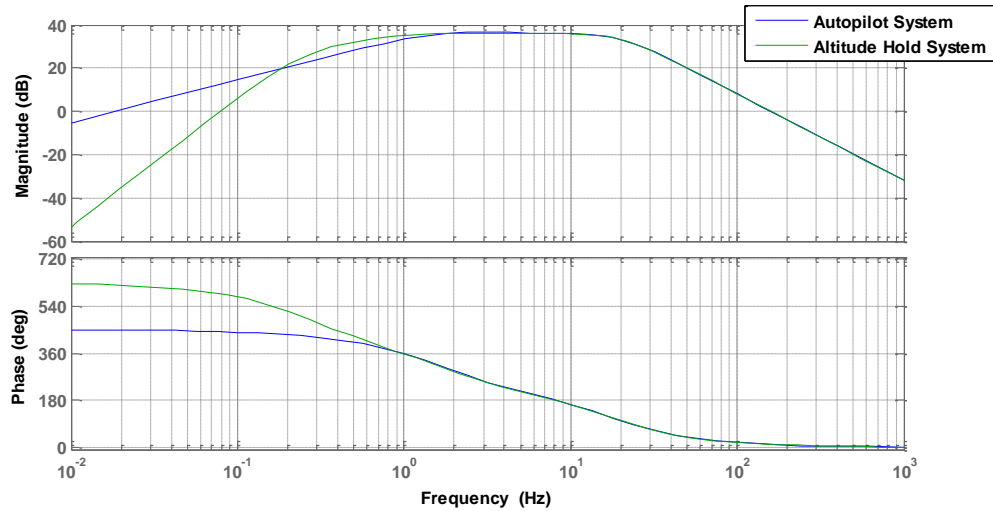


**Figure 2-23 Altitude Hold System frequency response for input disturbance**

As seen in Figure 2-23 at low frequencies disturbance rejection of Altitude Hold System is much better. Whereas input disturbance rejection performance of Altitude Hold System and Autopilot System becomes similar above frequency 0.2 Hz. It can be concluded that disturbance rejection performance is dominated by Autopilot System in the domain of frequencies near airframe natural frequency which is 1 Hz for Mach number 0.8. This conclusion is used for input design in Section 3.3.2.

For further analyses Altitude Hold Syste gains for Mach number 0.5 and 0.7 are calculated. Keeping transient performance characteristic similar selected gains for Mach number 0.5 and 0.7 are given in Table 2-9.

**Table 2-9 Altitude Hold System gains**

|  | Mach; 0.5 | Mach; 0.7 | Mach; 0.8 |
|---|---|---|---|
| K1 | 1.8 | 1.2 | 1 |
| K2 | 2.0 | 1.7 | 1.5 |

### 2.2.5.2  Inertial Measurement Unit

A MEMS based Inertial Measurement Unit (IMU) is modeled. IMU composed of a three axis accelerometer and gyro. The axial accelerations and angular rates are coming from flight mechanic as reference measurements. Noise, bias error and scale factor error are added to obtain IMU measurements. The block diagram of the IMU is shown in Figure 2-24.



(a)                                                      (b)
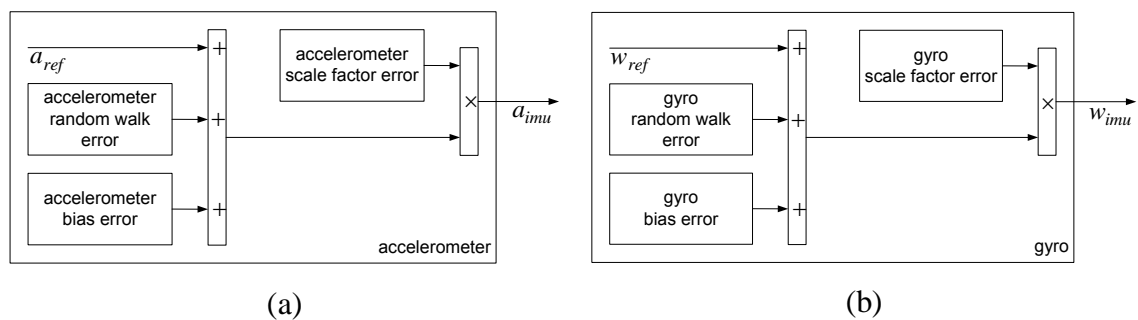
**Figure 2-24 IMU block diagrams, (a) Accelerometer, (b) Gyro**

It is assumed that IMU is placed at the center of gravity of the missile. So that IMU measurements are used without any transformation. If IMU is placed another location different from center of gravity one must transform the measurements before any estimation process. An example of the transformation of the IMU measurements is given in Section 3.5.1.

The typical error characteristics for MEMS based IMU are chosen for analyses. The magnitudes of errors are summarized in Table 2-10.

**Table 2-10 IMU noise characteristics**

|  | Acceloremeter | Gyro |
|---|---|---|
| Random Walk errror | 1 mg | 0.9 °/(h)$^{1/2}$ |
| Bias error | 40 mg | 150 °/h |
| Scale Factor error | 0.01 ppm | 0.01 ppm |

### 2.2.5.3 Control Actuation System

A Second Order non-linear actuator model is used for the Control Actuation System. The model is used directly from the library of MATLAB/Simulink. The damping ratio $\zeta$ and natural frequency $w_n$ are chosen as 0.7 and 20 Hz. The maximum deflection angle limit is 20° and maximum rate is 200°/s. The state space representation of Control Actuation System is given below.

$$\frac{\delta}{\delta_{com}} = \frac{w_n^2}{s^2 + 2\zeta w_n s + w^2} \tag{2-52}$$

$$\begin{bmatrix} \dot{\delta} \\ \ddot{\delta} \end{bmatrix} = \begin{bmatrix} 0 & 1 \\ -w_n^2 & -2\zeta w_n \end{bmatrix} \cdot \begin{bmatrix} \delta \\ \dot{\delta} \end{bmatrix} + \begin{bmatrix} 0 \\ w_n^2 \end{bmatrix} \cdot \delta_{com} \tag{2-53}$$

### 2.2.5.4 Turbojet Engine

Thrust of the missile is modeled as constant for desired Mach number. This causes that missile flight almost at constant speed at given altitude. Thrust direction is always in the x direction according to the inertial reference frame defined in the section 2.2.1 and directed through center of gravity of the missile. The analyses are done assuming that missile is flying at a trimmed level flight. The cruise speed is near 0.75 Mach. The speed of the missile is sustained applying constant thrust which is about 1375 N.

### 2.2.5.5 Mass Properties

Missile mass is modeled as given in various references defined in section 2.1. The moment inertia is modeled as assuming missile a cylinder rod. The center of gravity is chosen that 1.8 m from the nose which satisfies a good static margin. The mass properties used in the model are summarized in Table 2-11.

**Table 2-11 AGM-84A Harpoon Missile Model mass properties**

| $m$ | 515 kg |
|---|---|
| $I_y = I_z$ | 623.5 kg.m$^2$ |
| $I_x$ | 7.57 kg.m$^2$ |
| $c.g.$ location | 1.8 m (from nose) |

### 2.3 Simulation Results

In this section simulation results are discussed based on models discussed preceding sections. For the analyses a level flight at 200 m with cruise speed about 0.75 Mach is selected. The simulation results are given in Figure 2-25 Figure 2-26 Figure 2-27 and Figure 2-28. Note that missile flight about 200 m with a very little steady-state error with almost constant cruise speed. The angle of attack, pitch rate and control surface deflection are also constant. In other words missile flights in a level trimmed flight.
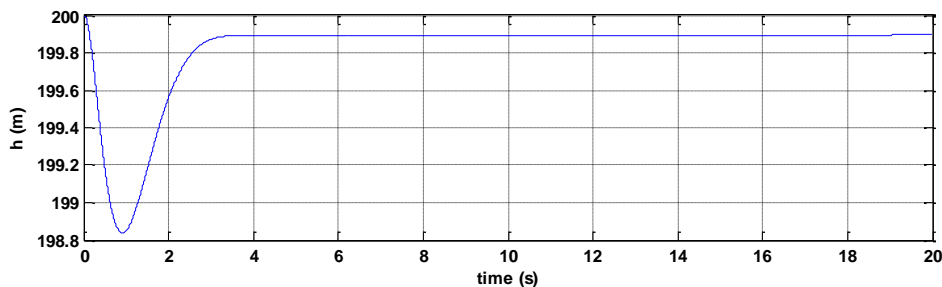


**Figure 2-25** *h* **versus time, Run-1**

43
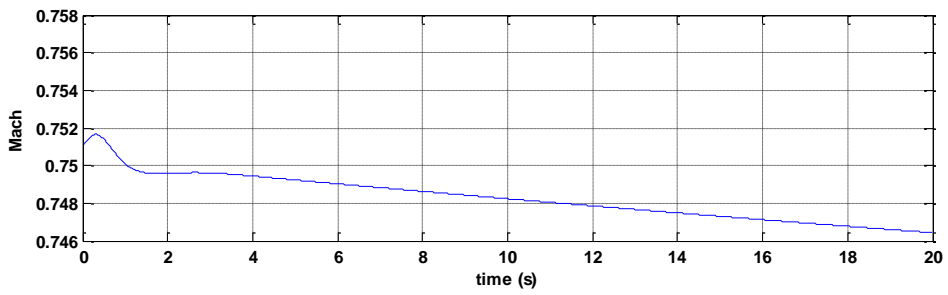
**Figure 2-26 Mach versus time, Run-1**
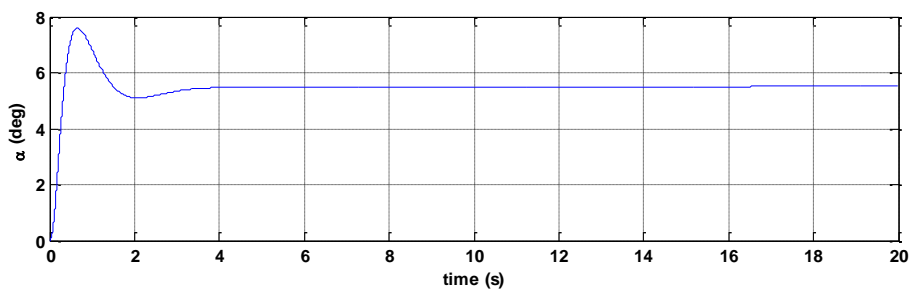


**Figure 2-27 $\alpha$ versus time, Run-1**
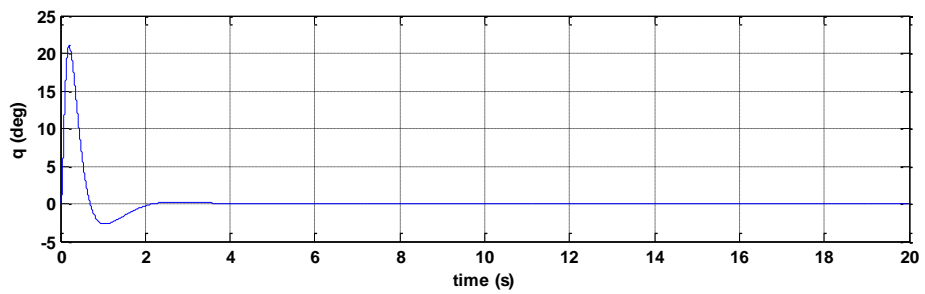


**Figure 2-28 $q$ versus time, Run-1**
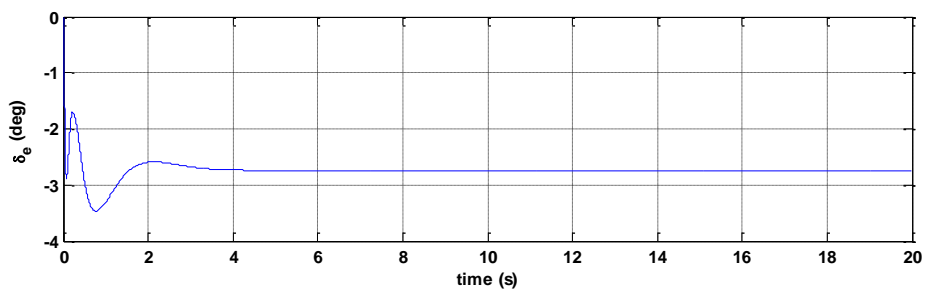


**Figure 2-29 $\delta_e$ versus time, Run-1**

44

# CHAPTER 3

# PARAMETER ESTIMATION

In this part of the thesis firstly parameter estimation techniques are presented. After that part input design procedure and estimation results are presented. Two different parameter estimation techniques are used. One of the techniques is ordinary least squares which is a time domain technique. The other is a frequency domain technique called equation error.

## 3.1 Ordinary Least Squares

Before starting estimation process the model equations must be defined. The model equations for the pitching moment coefficient and for the z force coefficient are defined as below.

$$C_z = C_{z_0} + C_{z_\alpha} \alpha + C_{z_\delta} \delta + C_{z_q} \frac{ql}{2V} \tag{3-1}$$

$$C_m = C_{m_0} + C_{m_\alpha} \alpha + C_{m_\delta} \delta + C_{m_q} \frac{ql}{2V} \tag{3-2}$$

Equations 3-1 and 3-2 can be generalized to the following model form for relating independent variables to a dependent variable [1].

$$y = \theta_0 + \sum_{j=1}^{n} \theta_j \xi_j \tag{3-3}$$

where $y$ is dependent variable, $\xi_j$ are linear or nonlinear functions of the $m$ independent variable $x_1, x_2, ..., x_m$; and the model parameters $\theta_0, \theta_1, \theta_2, ..., \theta_n$ are constants that quantify the influence of each term on the dependent variable $y$ [1]. The measured values of the dependent variable are corrupted by random measurement noise, so that

$$z(i) = \theta_0 + \sum_{j=1}^{n} \theta_j \xi_j(i) + v(i) \qquad i = 1, 2, ..., N \qquad (3\text{-}4)$$

where $z(i)$ are the output measurements, $N$ is the number of data points, and the $\xi_j(i)$ depend on the $m$ independent variables $x_1, x_2, ..., x_m$ at the $i$ th data point. Equation 3-4 is called regression equation and $\xi_j$, $j = 1, 2, ..., n$ called regressors [1].

Equation 3-3 and 3-4 can be written using vector and matrix notation as

$$y = X\theta \qquad (3\text{-}5)$$

$$z = X\theta + v \qquad (3\text{-}6)$$

where

$z = \begin{bmatrix} z(1) & z(2) & ... & z(N) \end{bmatrix}^T = N \times 1$ vector

$\theta = \begin{bmatrix} \theta_0 & \theta_1 & ... & \theta_n \end{bmatrix}^T = n_p \times 1$ vector of unknown parameters, $n_p = n + 1$

$X = \begin{bmatrix} 1 & \xi_1 & ... & \xi_n \end{bmatrix}^T = N \times n_p$ matrix of vectors of ones and regressors

$v = \begin{bmatrix} v(1) & v(2) & ... & v(N) \end{bmatrix}^T = N \times 1$ vector of measurements errors

The best estimator $\theta$ in a least square sense comes from minimizing the sum of squared differences between the measurements and the model

$$J(\theta) = \frac{1}{2}(z - X\theta)^T (z - X\theta) \qquad (3\text{-}7)$$

$$\hat{\theta} = \min_{\theta} \frac{1}{2}(z - X\theta)^T (z - X\theta) \qquad (3\text{-}8)$$

$$\frac{\partial J}{\partial \theta} = -X^T z + X^T X \hat{\theta} = 0 \qquad (3\text{-}9)$$

$$X^T X \theta = X^T z \qquad (3\text{-}10)$$

$$X^T (z - X\hat{\theta}) = 0 \qquad (3\text{-}11)$$

The ordinary least-squares estimator is obtained as

$$\hat{\theta} = (X^T X)^{-1} X^T z \qquad (3\text{-}12)$$

Remembering model equations defined in the Equation 3-1 and 3-2, elements in the ordinary least-squares estimator for the z force are as follows;

$1 \times 4$ parameter vector is
$$\hat{\theta} = \begin{bmatrix} C_{z_0} & C_{z_\alpha} & C_{z_\delta} & C_{z_q} \end{bmatrix}^T$$

$N \times 4$ regressors matrix is
$$X = \begin{bmatrix} 1 & \alpha(1) & \delta_e(1) & \frac{l}{2V}q(1) \\ 1 & \alpha(2) & \delta_e(2) & \frac{l}{2V}q(2) \\ \vdots & \vdots & \vdots & \vdots \\ 1 & \alpha(N) & \delta_e(N) & \frac{l}{2V}q(N) \end{bmatrix}$$

$1 \times N$ measurement vector is
$$z = \begin{bmatrix} C_z(1) & C_z(2) & \cdots & C_z(N) \end{bmatrix}^T$$

The elements $\delta_e$ and $q$ in the regressors matrix is obtained sensor measurements in Control Actuation System model and IMU model. Angle of attack $\alpha$ measurement is obtained from Inertial Navigation System model using Equation 2.23. Note that pitch rate is multiplied by characters length $l$ and divided by instantaneous velocity as in the model equation. The elements in the measurement vector are calculated from non-dimensionalized z force which is obtained by product of mass and axial acceleration in z direction given Equation 3-13. Remember that acceleration in z direction is output of accelerometer in IMU model. Note that IMU modeled in the flight simulation measures only reaction force which corresponds to only aerodynamic force in air.

$$F_z = ma_z \tag{3-13}$$

$$C_z = \frac{F_z}{QS} \tag{3-14}$$

For the pitching moment equation defined in Equation 3-2, the elements in the least-squares estimators are as follows;

$1 \times 4$ parameter vector is $\quad \hat{\theta} = \begin{bmatrix} C_{m_0} & C_{m_\alpha} & C_{m_\delta} & C_{m_q} \end{bmatrix}^T$

$N \times 4$ regressors matrix is $\quad X = \begin{bmatrix} 1 & \alpha(1) & \delta_e(1) & \frac{l}{2V}q(1) \\ 1 & \alpha(2) & \delta_e(2) & \frac{l}{2V}q(2) \\ \vdots & \vdots & \vdots & \vdots \\ 1 & \alpha(N) & \delta_e(N) & \frac{l}{2V}q(N) \end{bmatrix}$

$1 \times N$ measurement vector is $\quad z = \begin{bmatrix} C_m(1) & C_m(2) & \cdots & C_m(N) \end{bmatrix}^T$

The elements in the regressor matrix of pitching moment are calculated as defined for the regressor matrix of z force. The measurement vector elements are obtained by Equation 2-17. Since missile is a rigid body and symmetric in the pitch and yaw plane $I_{xz} = 0$. Then Equation 2-17 becomes,

$$\dot{q} = \frac{QSl}{I_y} C_m - \frac{(I_x - I_z)}{I_y} pr \tag{3-15}$$

$$C_m = \frac{\dot{q} I_y + (I_x - I_z) pr}{QSl} \tag{3-16}$$

As seen from Equation 3-15 first-time derivative of pitch rate must be obtained. Pitch rate is obtained as gyro measurement from IMU model. Since it is noisy data it must be filtered before derivation process. The details of the filter used in the thesis are given in Section 3.4.1.

In the estimation process the statistical process of least-squares estimator are widely used. These properties determine whether postulated model is good enough to define the measurement or highlight near-linear correlation among the regressors.

Remember that least-squares estimates focuses on minimizing sum of squared differences between model and measurement. Then the covariance matrix for parameter estimate $\hat{\theta}$ is found by estimate error which is difference between parameter estimate and true parameter vector $\theta$.

$$Cov(\hat{\theta}) = E\left[(\hat{\theta} - \theta)(\hat{\theta} - \theta^T)\right] \tag{3-17}$$

using Equation 3-5 and 3-6, Equation 3-17 becomes

$$E\{(X^T X)^{-1} X^T (z - y)(z - y)^T X (X^T X)^{-1}\} \tag{3-18}$$

$$(X^TX)^{-1}X^TE(vv^T)X(X^TX)^{-1} \tag{3-19}$$

making the assumption that measurement error are uncorrelated and have constant variance, $E(vv^T) = \sigma^2 I$, Equation 3-17 becomes

$$Cov(\hat{\theta}) = E\left[(\hat{\theta} - \theta)(\hat{\theta} - \theta)^T\right] = \sigma^2(X^TX)^{-1} \tag{3-20}$$

Defining the matrix $(X^TX)^{-1}$ as $\left[d_{jk}\right]$ where $j,k = 1,2,...,n_p$, the variance of the $j$th diagonal element of the covariance matrix,

$$Var(\hat{\theta}_j) = \sigma^2 d_{jj} \qquad\qquad j,k = 1,2,...,n_p \tag{3-21}$$

and the covariance between two estimated parameters $\hat{\theta}_j$ and $\hat{\theta}_k$ is

$$Cov(\hat{\theta}_j, \hat{\theta}_k) = \sigma^2 d_{jk} \qquad\qquad j,k = 1,2,...,n_p \tag{3-22}$$

The correlation coefficient $r_{jk}$ is defined as

$$r_{jk} \equiv \frac{d_{jk}}{\sqrt{d_{jj}d_{kk}}} = \frac{Cov(\hat{\theta}_j, \hat{\theta}_k)}{\sqrt{Var(\hat{\theta}_j)Var(\hat{\theta}_k)}} \qquad\qquad j,k = 1,2,...,n_p \tag{3-23}$$

$$-1 \leq r_{jk} \leq 1 \qquad\qquad j,k = 1,2,...,n_p \tag{3-24}$$

The correlation coefficient $r_{jk}$ is a measure of the pair-wise correlation between parameter estimates $\hat{\theta}_j$ and $\hat{\theta}_k$ [1]. A value of $\left|r_{jk}\right| = 1$ means that estimated parameters $\hat{\theta}_j$ and $\hat{\theta}_k$ are linearly dependent or, equivalently, that their corresponding regressors are linearly dependent [1]. Arranging all the values of

$r_{jk} = 1$ in an $n_p \times n_p$ matrix forms the parameter correlation matrix which is symmetric with ones on the main diagonal.

Standard errors for the parameter estimates are computed from the square root of the diagonal elements of the covariance matrix given in Equation 3-20.

t statistics indicates the significance of the parameter in the model equations. It is computed by the ratio of parameter estimates to standard error given in Equation 3-25.

$$t_0 = \frac{\hat{\theta}_i}{s(\hat{\theta}_i)} \qquad i = 1,2,...,n_p \qquad (3\text{-}25)$$

Another statistical metric that defines the closeness of the model to measurement is the coefficient of determination $R^2$. The coefficient of determination is the ratio of the regression sum of squares $SS_R$ to total sum of squares $SS_T$. The total sum of squares is the sum of squared variations in the measured output about its mean value. And the regression sum of squares is the sum of squared variations of the model about the same mean value.

$$\bar{z} = \frac{1}{N} \sum_{i=1}^{N} z(i) \qquad (3\text{-}26)$$

$$SS_T \equiv \sum_{i=1}^{N} [z(i) - \bar{z}]^2 \qquad (3\text{-}27)$$

$$SS_R \equiv \sum_{i=1}^{N} [y(i) - \bar{z}]^2 \qquad (3\text{-}28)$$

$$R^2 = \frac{SS_R}{SS_T} \qquad (3\text{-}29)$$

## 3.2 Complex Linear Regression

The parameter estimation can also be done in frequency domain. Frequency domain analysis has certain advantages, including physical insight in terms of frequency content, direct applicability to control system design, and a smaller number of data points for parameter estimation, among others [1].

Frequency domain methods are built on finite Fourier transformation, which convert data from time domain to frequency domain. Time domain data is converted to the frequency domain via Fourier Integral. For a given continuous function in the time domain $x(t)$, the corresponding continuous function in the frequency domain $x(\tilde{w})$ is obtained as

$$F[x(t)] \equiv x(\tilde{w}) = \int_{-\infty}^{\infty} x(t)e^{-jwt}dt \qquad (3\text{-}30)$$

Where $j = \sqrt{-1}$ and $w$ is the angular frequency in radians per second. Transformation properties are discussed in detail in many references.

Linear regression in the frequency domain follows the same approach as the time domain which details are given in section 3.1.

$$z = X\theta + v \qquad (3\text{-}31)$$

where

$\tilde{z} = N \times 1$ vector of transformed dependent variable measurements

$\theta = n_p \times 1$ vector of unknown parameters, $n_p = n + 1$

$\tilde{X} = N \times n_p$ matrix of vectors of ones and transformed regressors

$\tilde{v} = N \times 1$ vector of complex measurements errors

The best estimator $\theta$ in a least square sense comes from minimizing Equation 3-32

$$J(\theta) = (\tilde{z} - \tilde{X}\theta)^{\dagger}(\tilde{z} - \tilde{X}\theta) \qquad (3\text{-}32)$$

which results in the least-squares estimate

$$\hat{\theta} = [\tilde{X}^{\dagger}\tilde{X}]^{-1}\tilde{X}^{\dagger}\tilde{z} \qquad (3\text{-}33)$$

## 3.3 Open Loop Parameter Estimation from Closed Loop Data

Parameter estimation under continuously operating feedback control system presents new challenges to the estimation field. The excitation given to the system is understood by the system as disturbance that should be damped or eliminated [1]. This elimination causes to mute natural dynamic response of the system. In addition to that the movement of control surfaces by feedback control causes high correlation with one other or with state variables [1] which is called data collinearity. In order to increase the performance of estimation process data collinearity must be analyzed and reduced.

Data collinearity problem can be solved through the modeling process, by estimating equivalent derivatives, or by using biased estimators [1]. Other and probably the best choice to reduce data collinearity is better system excitation [2] which is done by adding separate surface inputs to the control actuation system while feedback control system is operating. This can be done within the flight computer. A schematic diagram of applying separate surface inputs is shown below.
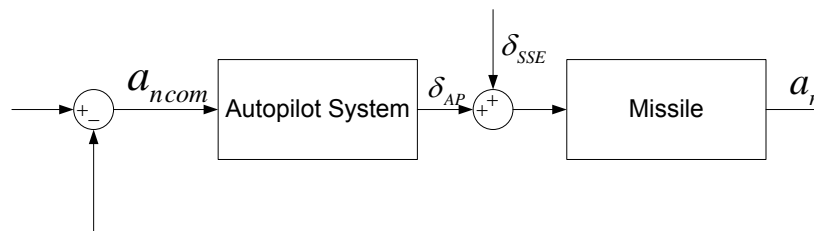


**Figure 3-1 Separate surface excitation addition**

The design of SSE is an important issue to reduce data collinearity and increase parameter estimation performance. The amplitude and period of the SSE must be selected systematically and a data collinearity check must be done.

Before beginning input design and estimation process in this thesis following assumptions are made.

- A priori information about the system is known. In other words there is a priori information or initial guess exist like airframe natural frequency or system linear boundaries

- This priori information about the system is used as start point in Input Design process

### 3.3.1  Input Design

One of the focuses of this work is to design the input in a systematic manner. To do this firstly closed system must be analyzed. Then input signal is selected considering the following issues.

- measured output signal to noise ratio

- mission performance and autopilot limits

- data collinearity

A proposed input design procedure is shown in the Figure 3-2.
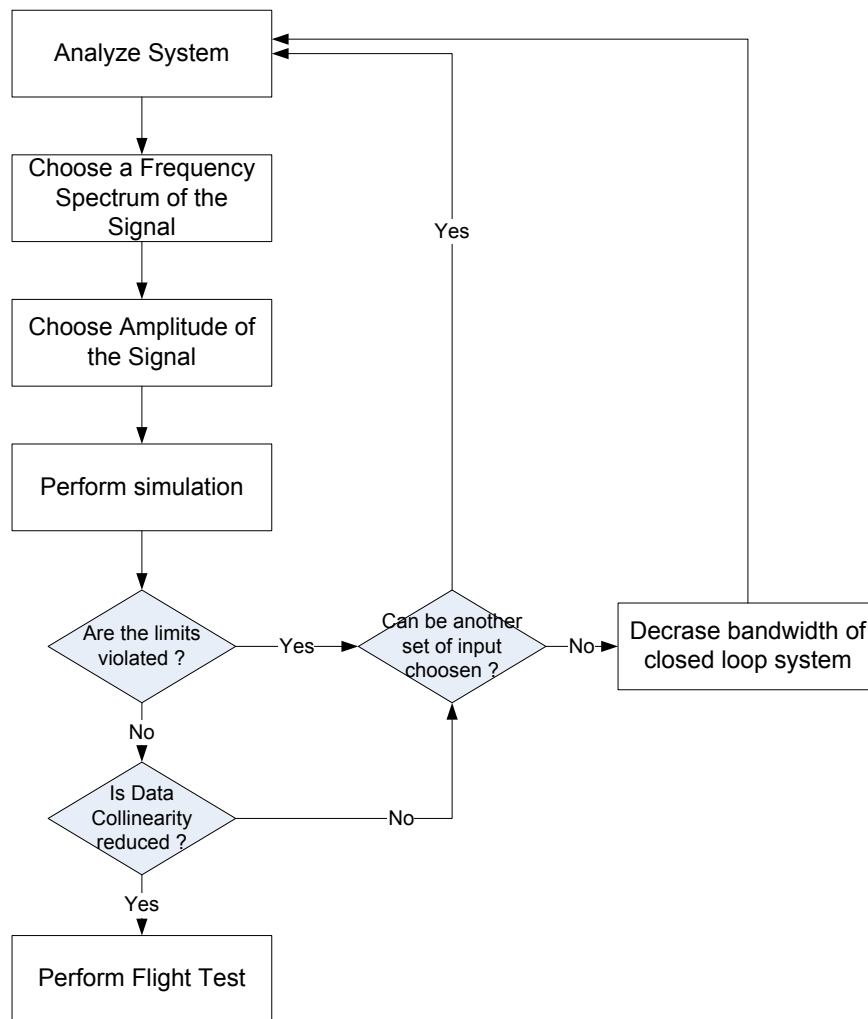
**Figure 3-2 Input Design procedure**

The procedure starts by analyzing the closed loop system, which helps with the selection of a suitable frequency spectrum and amplitude for the input signal. In this stage one must assure that closed loop system limits such as linear region for the autopilot or the mission performance of the system are not violated. The next selection criterion is collinearity reduction. In order to get good estimation result data collinearity must be reduced to acceptable levels. If these criteria are not satisfied try to change the frequency spectrum or amplitude of the signal. If there is no solution exists that does not violate closed loop limits, decreasing the bandwidth of the closed loop system must be taken into consideration.

### 3.3.2 Analysis of the System

As mentioned in the previous section closed loop system must be analyzed firstly. The frequency response analysis of the closed loop system is a good starting point. The frequency response for Mach number 0.8 of closed loop system from control surface command to normal acceleration is given Figure 3-3.
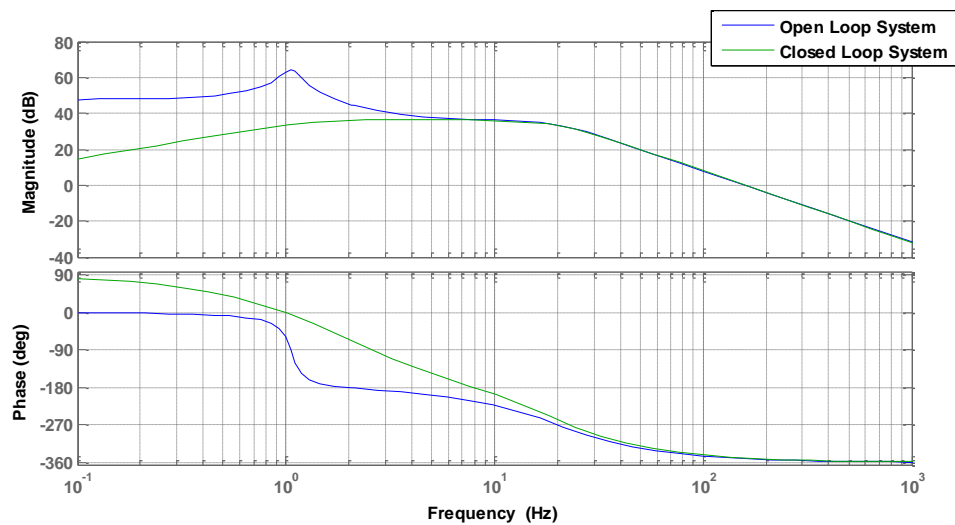


**Figure 3-3 Open & Closed Loop System frequency response**

Note that below frequencies 1 Hz, the output of closed loop system is much more damped by feedback controller. As the frequency increases above 5 Hz, the closed loop system behaves like the open loop system which means that closed loop system bandwidth is reached. In our case choosing an input signal which has a power spectrum signal from 0.9 Hz to 1.1 Hz is good enough to collect necessary information for estimation. Remember that as Mach number decreases natural airframe frequency also decreases. Since missile flight in a trimmed level flight condition about Mach number 0.75. It is wisely to include frequency spectrum below 1 Hz to the input signal.

The amplitude of the input signal must be selected considering limits of the closed loop system. Remember that a linear region is defined for the autopilot of the system.

So after applying the selected input signal to the system, the system must be within defined linear region of the system which is ±10° for angle of attack and control surface deflection. Another violation criterion may come from the mission profile of the missile. It can be said that the altitude must remain ±10 m region while applying the input signal. The amplitude range can be seen from the bode diagram of closed loop system from control surface input to angle of attack. For Mach number 0.8 the bode diagram is given below.
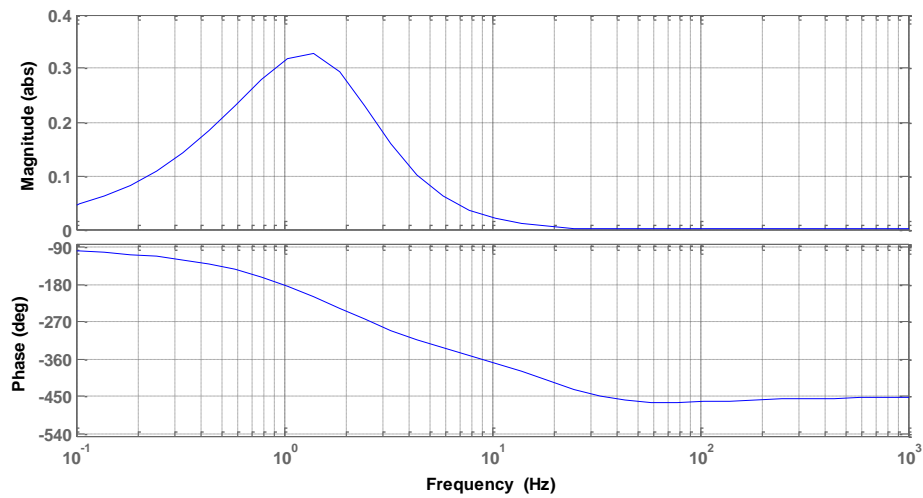


**Figure 3-4 Closed Loop System frequency response of from $\delta_e$ to $\alpha$**

It can be seen that for 1° control surface input 0.327° angle of attack occurs at about 1 Hz. Since at trim the missile flies at about 5° angle of attack and -3° elevator command, there is a margin for staying in the linear region of the system. The amplitude must be chosen considering mission profile limitation.

A stacked sine wave input signal is chosen as defined in Equation 3-35. A is the amplitude of the signal and B1 and B2 are the frequencies of the sine wave.

$$\delta_{SSE} = A[\sin(2\pi B1 t) + \sin(2\pi B2 t)] \tag{3-34}$$

57

Amplitude of the input signal A is chosen as -3°, and frequencies of the signal B1 are selected as 0.9 Hz and 1.1 Hz. The violation limits must be controlled in order to continue input selection procedure. Suppose a level trimmed flight occur at altitude 200 m. Altitude, cruise velocity, angle of attack, pitch rate and control surface command are given in Figure 3-5, Figure 3-6, Figure 3-7, Figure 3-8 and Figure 3-9.
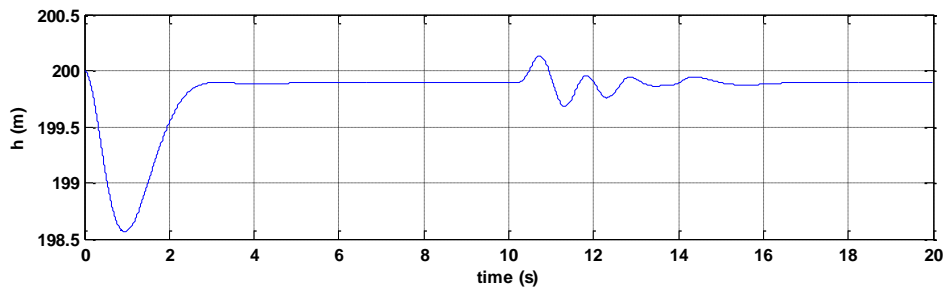


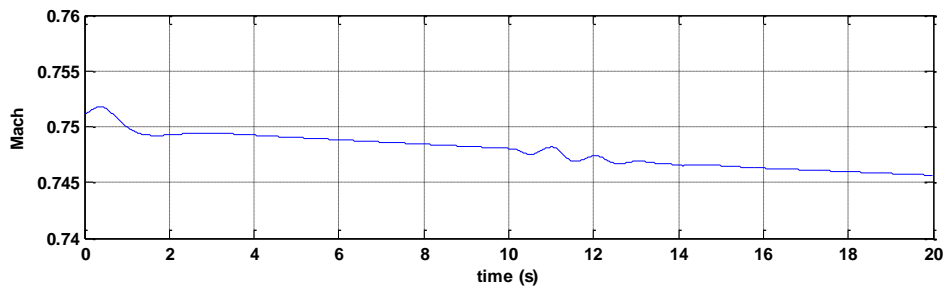**Figure 3-5** *h* **versus time, Run-2**



**Figure 3-6 Mach versus time, Run-2**
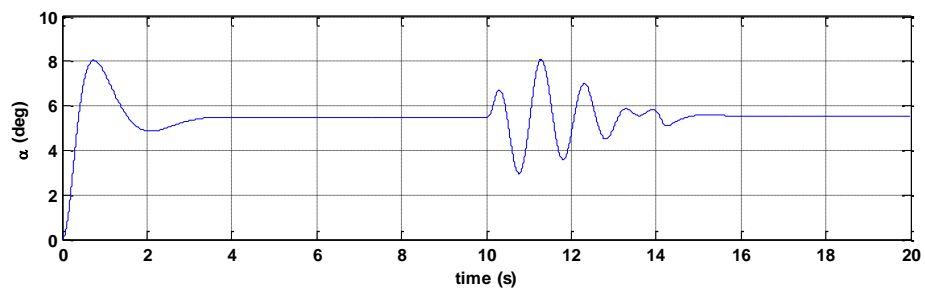


**Figure 3-7** *α* **versus time, Run-2**
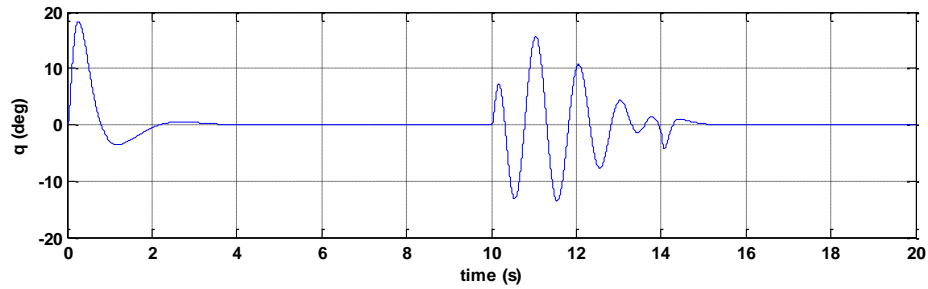
**Figure 3-8** $q$ **versus time, Run-2**
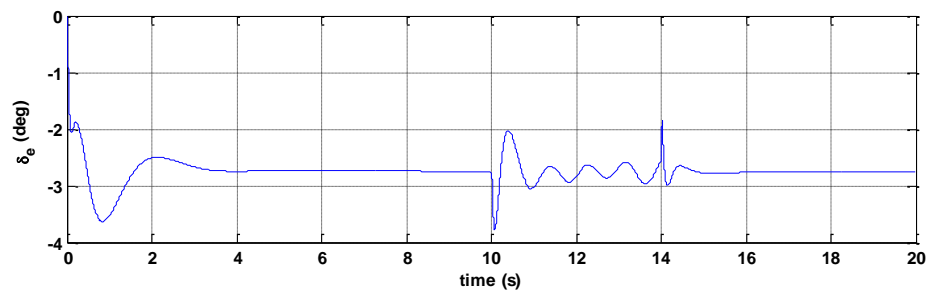


**Figure 3-9** $\delta_e$ **versus time, Run-2**

Note that the excitation input does not violate the limits of the closed loop system. The closed loop system remains in linear region. In addition to that the mission profile is also in limit values. The selected signal can be used for further analyses.

### 3.3.3 Data Collinearity

As pointed earlier the separate surface excitations must be chosen carefully to reduce correlation between data. Since the system is a single input system, correlation occurs between states of the missile. The correlation can be easily seen from graphs of states between each other. For time from 0 s to 4 s the correlation figure between delta and angle of attack is given in Figure 3-10. Note that there is a linear relationship between elevator command angle of attack. Figure 3-11 shows delta versus alpha between 10 s and 14 s where SSE is applied. As seen from the figure there is no linear relationship between elevator command and angle of attack. In other words these two states are uncorrelated in that region.

59
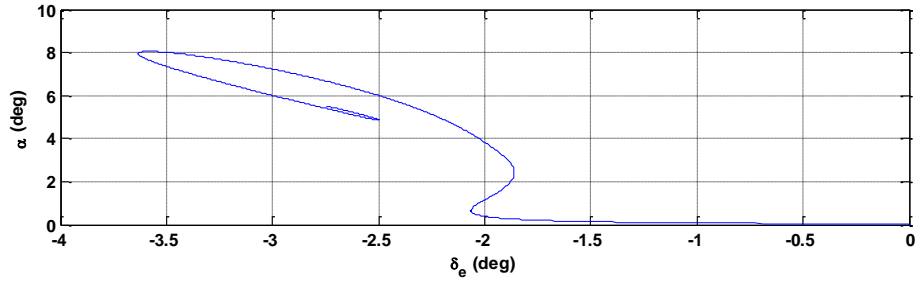
**Figure 3-10** $\delta_e$ **versus** $\alpha$ **without SSE, correlated**
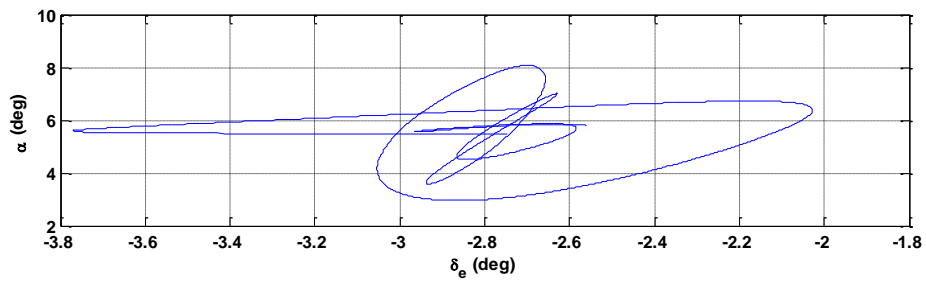


**Figure 3-11** $\delta_e$ **versus** $\alpha$ **with SSE, uncorrelated**

Several techniques are available to measure correlation between variables such as examination of the regressor correlation matrix and its inverse, eigensystem analysis and parameter variance decomposition. Details of these techniques and some other techniques can be found in [1, 2]. In this thesis data collinearity check is done through examination of the regressor correlation matrix. The regressor correlation matrix is derived from least squares estimator. The detail of ordinary least squares estimator is given in section 3.1.

Using the correlation information different set of inputs which satisfies correlation criteria can be designed. A rule of thumb is that the absolute value of elements of correlation matrix must be below 0.9 [1].

For time from 0 s to 4 s the correlation matrix for the normal force model equation $C_z = C_{z_0} + C_{z_\alpha} \alpha + C_{z_\delta} \delta + C_{z_q} \dfrac{ql}{2V}$ is found as below.

**Table 3-1 Parameter correlation matrix (0-4s), Run-2**

|  | $C_{z_\alpha}$ | $C_{z_\delta}$ | $C_{z_q}$ |
|---|---|---|---|
| $C_{z_\alpha}$ | 1 | -0.9215 | -0.3380 |
| $C_{z_\delta}$ | - | 1 | 0.4256 |
| $C_{z_q}$ | - | - | 1 |

As seen from Table 3-1 a high correlation exists between angle of attack and elevator command. After applying SSE the correlation matrix becomes as below.

**Table 3-2 Parameter correlation matrix (10-14s), Run-2**

|  | $C_{z_\alpha}$ | $C_{z_\delta}$ | $C_{z_q}$ |
|---|---|---|---|
| $C_{z_\alpha}$ | 1 | 0.2930 | 0.0871 |
| $C_{z_\delta}$ | - | 1 | -0.4175 |
| $C_{z_q}$ | - | - | 1 |

The implementation of SSE successfully reduces data collinearity as expected. The same results occur for the pitching moment model equation $C_m = C_{m_0} + C_{m_\alpha} \alpha + C_{m_\delta} \delta + C_{m_q} \dfrac{ql}{2V}$ since pair-wise correlation between parameter estimates $\hat{\theta}_j$ and $\hat{\theta}_k$ is equal to their corresponding regressors $\alpha$, $\delta$ and $q$.

**Table 3-3 Parameter correlation matrix (0-4s), Run-2**

| | $C_{m_\alpha}$ | $C_{m_\delta}$ | $C_{m_q}$ |
|---|---|---|---|
| $C_{m_\alpha}$ | 1 | -0.9215 | -0.3380 |
| $C_{m_\delta}$ | - | 1 | 0.4256 |
| $C_{m_q}$ | - | - | 1 |

**Table 3-4 Parameter correlation matrix (10-14s), Run-2**

| | $C_{m_\alpha}$ | $C_{m_\delta}$ | $C_{m_q}$ |
|---|---|---|---|
| $C_{m_\alpha}$ | 1 | 0.2930 | 0.0871 |
| $C_{m_\delta}$ | - | 1 | -0.4175 |
| $C_{m_q}$ | - | - | 1 |

The ratio of reducing data collinearity depends on the characteristics of the chosen SSE signal. The type, period and amplitude of the signal affect directly data correlation. To illustrate this at a constant amplitude sine signal is applied as SSE at increasing frequencies between 10 s - 14 s. For the chosen -3 deg amplitude, changes of correlation numbers are summarized in Table 3-5.

**Table 3-5 Parameter correlation change increasing SSE frequency**

| | No Input | 0.5 Hz | 1 Hz | 10 Hz |
|---|---|---|---|---|
| $\alpha$ - $\delta_e$ | 1 | 0.9556 | 0.4463 | 0.6997 |
| $\alpha$ - $q$ | 0.9997 | 0.2343 | 0.0873 | 0.1309 |
| $\delta_e$ - $q$ | 0.9997 | 0.4169 | 0.5882 | 0.7883 |

Note that correlation of states decrease until frequency 1 Hz and then slightly increases. This is due to that maximum response is taken to applied input at natural

aerodynamic frequency of the airframe. Similar analysis is made for find the effect of the amplitude of the SSE. To do this a sine signal is selected as SSE with frequency 1 Hz. The results are given in Table 3-6. Note that with increasing amplitude of the SSE, data collinearity between states decreases. This can be explained by the increase of observability of the states. In other words change in the states is much more observable which results in high signal to noise ratio. This situation becomes more important in case of noisy sensor measurements or turbulent flight conditions.

**Table 3-6 Parameter correlation change increasing SSE amplitude**

|  | No Input | -0.5 deg | -3 deg | -4 deg |
|---|---|---|---|---|
| $\alpha - \delta_e$ | 1 | 0.4848 | 0.4463 | 0.2724 |
| $\alpha - q$ | 0.9997 | 0.0863 | 0.0873 | 0.0874 |
| $\delta_e - q$ | 0.9997 | 0.5734 | 0.5882 | 0.4469 |

## 3.4 Parameter Estimation Results

In this part parameter estimation is done using inputs designed by procedure defined in Section 3.3.1. The results are compared with each other and with the simulation database.

### 3.4.1 Ordinary Least Squares Estimation Results

In this part of thesis normal force and pitching moment derivatives are estimated using ordinary least squares estimation technique. The SSE input is stacked sine wave which is in the form $\delta_{SSE} = A[\sin(2\pi B1t) + \sin(2\pi B2t)]$. Using the input design procedure in section 3.3.1, amplitude is selected as -3 deg, B1 as 0.9 Hz and B2 as 1.1 Hz. The model fit is given in Figure 3-12. As seen from the figure model fit is good enough and residuals are almost randomly distributed which means that model fit error is very small.
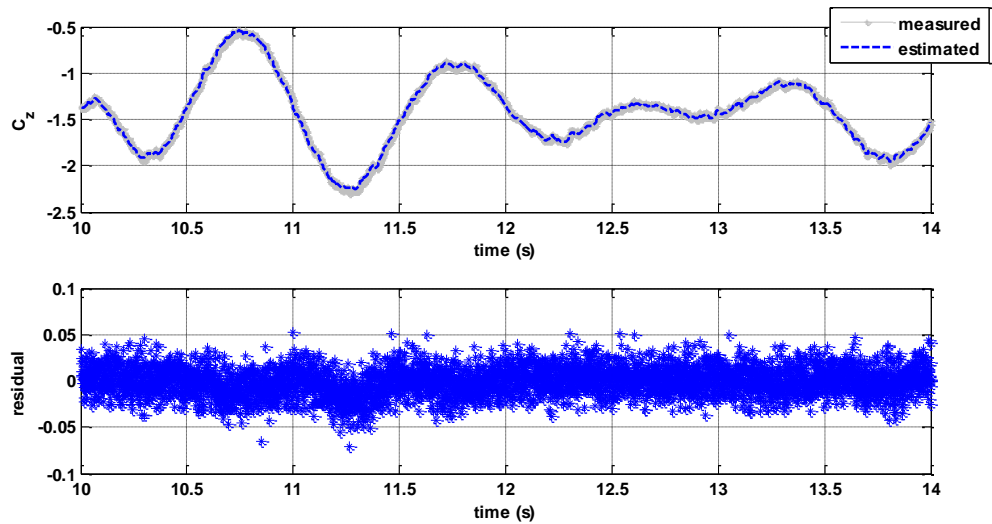
**Figure 3-12 Least Squares model fit to $C_z$ and Residuals**

The estimation results are summarized in Table 3-7. The estimation statistics shows that model parameters has good significance ratio compared to each other. On the other hand fit error and standard errors are very small.

**Table 3-7 Least Squares parameter estimation results, $C_z$**

|  | $\hat{\theta}$ | $s(\hat{\theta})$ | $|t_0|$ | $100\left[s(\hat{\theta})/|\hat{\theta}|\right]$ |
|---|---|---|---|---|
| $C_{z_0}$ | 0.0814 | 0.0012 | 67.83 | 1.47 |
| $C_{z_\alpha}$ | -19.187 | 0.0052 | 3689.8 | 0.03 |
| $C_{z_\delta}$ | -7.2856 | 0.0185 | 393.81 | 0.25 |
| $C_{z_q}$ | -112.3293 | 1.3032 | 86.19 | 1.16 |
| $s = \hat{\sigma}$ | 0.006 |  |  |  |
| $R^2, \%$ | 0.9998 |  |  |  |

Using the estimation results one can calculate local aerodynamic coefficient curve since aerodynamic curves are almost linear in the estimation region. The calculated

local aerodynamic curve and true aerodynamic curve are given in Figure 3-13. As seen from the figure estimation results are very close to the aerodynamic database.
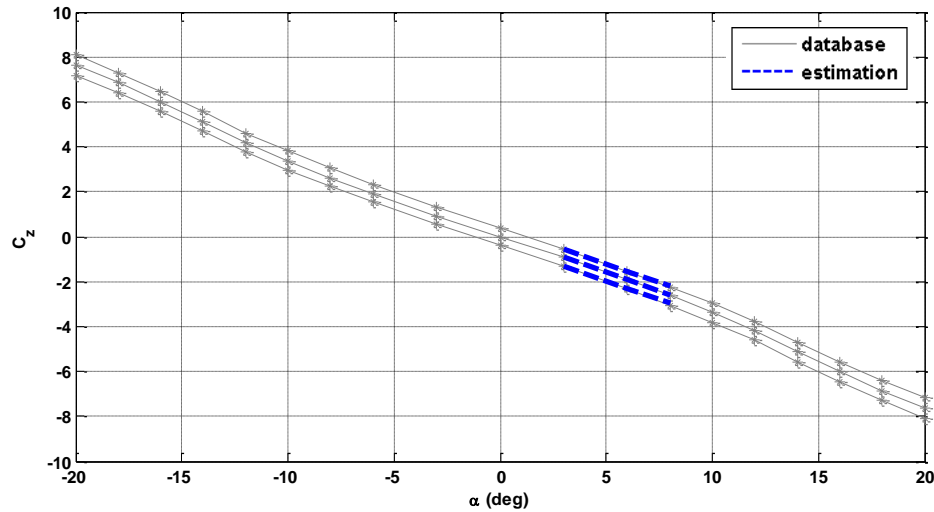


**Figure 3-13 Local estimation result,** $C_z$

Besides graphical comparison the estimation values are also compared with the true values. The coefficient values of aerodynamic database are obtained from local slope of $C_z$-$\alpha$ and $C_z$-$\delta$ curves. Dynamic coefficient value is obtained by interpolation from dynamic coefficient database. The comparison is given in Table 3-8.

**Table 3-8 Aerodynamic database and estimation results**

|  | Real Value | $\hat{\theta}$ | % Error |
|---|---|---|---|
| $C_{z_\alpha}$ | -19.6295 | -19.187 | 2.25 |
| $C_{z_\delta}$ | -7.41 | -7.2856 | 1.67 |
| $C_{z_q}$ | -113.575 | -112.3293 | 1.09 |

Before estimating pitching moment, pitching moment measurement must be obtained from noisy data. Since pitch rate is a noisy measurement it must be filtered to find its

derivative. Various filtering techniques are available in the literature. One of the approaches is global Fourier smoothing. Detail of the technique can be found in reference [1]. Before estimating pitch moment coefficients pitch rate is filtered. Original pitch rate and filtered pitch rate are shown in Figure 3-14. Note that if filter cut-off frequency chosen very low the behavior of the original signal is lost. So that 10 Hz is selected as cut-off frequency which filters noise with high frequency component without losing the behavior of the signal.
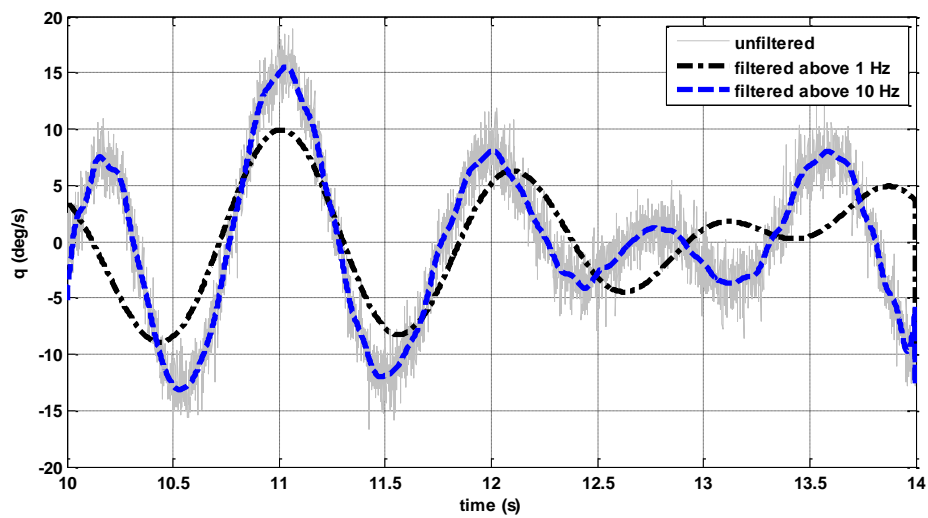


**Figure 3-14 Global Fourier Smoothing of pitch rate**

Pitching moment model fit and residuals are given in Figure 3-15. As seen from the figure residuals are small, and almost randomly distributed. In other words measurement is well defined by the model.
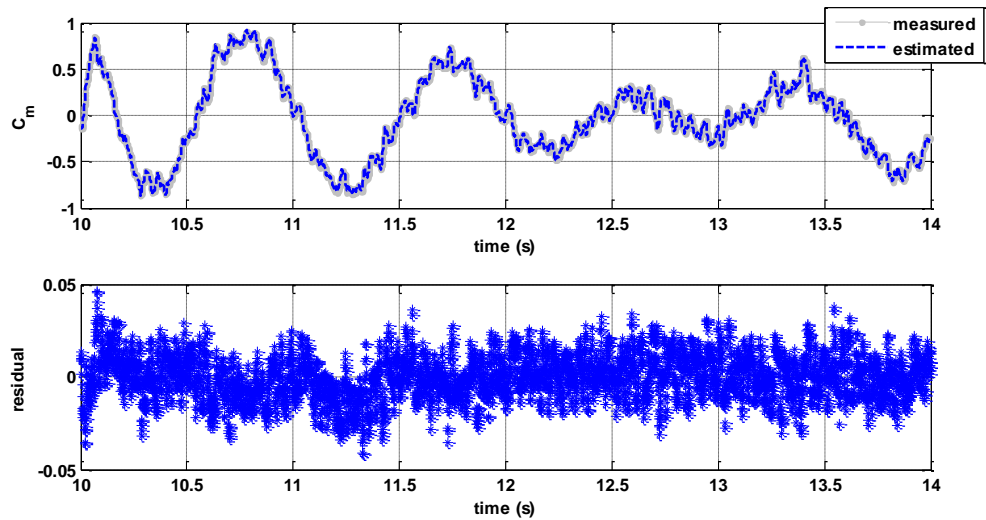
**Figure 3-15 Least Squares model fit to $C_m$ and Residuals**

Pitching moment estimation results are given in Table 3-9. As seen from the table model parameters significances are close relative to each other and standard errors are small.

**Table 3-9 Least Squares parameter estimation results, $C_m$**

|  | $\hat{\theta}$ | $s(\hat{\theta})$ | $|t_0|$ | $100\left[s(\hat{\theta})/|\hat{\theta}|\right]$ |
|---|---|---|---|---|
| $C_{m_0}$ | -0.1526 | 0.0024 | 63.58 | 1.572 |
| $C_{m_\alpha}$ | -16.5539 | 0.011 | 1504.9 | 0.066 |
| $C_{m_\delta}$ | -36.2128 | 0.0383 | 945.5 | 0.105 |
| $C_{m_q}$ | -429.6092 | 2.739 | 156.85 | 0.64 |
| $s = \hat{\sigma}$ | 0.0126 |  |  |  |
| $R^2, \%$ | 0.9991 |  |  |  |

Graphical comparison is made for pitching moment using the estimated values. The result is given in Figure 3-16. As seen from the figure the estimation results are not

as close as the normal force coefficient. One portion of the error comes from filtering pitch rate because some delay and information loss comes to the data. Despite this error the results are still close to the aerodynamic database.
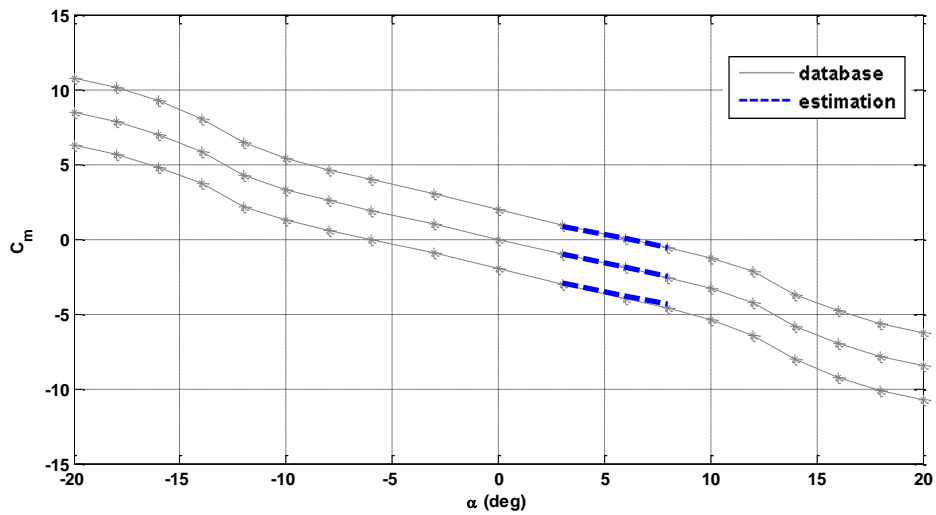


**Figure 3-16 Local estimation result, $C_m$**

The numeric comparison is given in Table 3-10.The coefficient values of aerodynamic database are obtained from local slope of $C_m$-$\alpha$ and $C_m$-$\delta$ curves. Dynamic coefficient value is obtained by interpolation from dynamic coefficient database.

**Table 3-10 Aerodynamic database and estimation results**

|  | Real Value | $\hat{\theta}$ | % Error |
|---|---|---|---|
| $C_{m_\alpha}$ | -17.544 | -16.5539 | 5.64 |
| $C_{m_\delta}$ | -37.3716 | -36.2128 | 3.21 |
| $C_{m_q}$ | -439.83 | -429.6092 | 2.3 |

### 3.4.2 Complex Linear Regression Estimation Results

In order to complex linear regression measurement obtained in time domain must be transformed in to the frequency domain. The transformation is done by using Equation 3-30 for a selected frequency range. The transformation frequency range is selected between 0.05 Hz to 10 Hz. Note that the measured motions of the missile are within the selected range and components with high frequency components like sensor measurements are neglected. In the algorithm parameter estimation is made recursively. In the first second data is collected. After that every 200 ms a new update in parameter estimation is made.

For the data obtained in Section 3.1 the aerodynamic coefficients are re-calculated in the frequency domain. The graphical representation of calculations is given in Figure 3-17, Figure 3-18 and Figure 3-19.
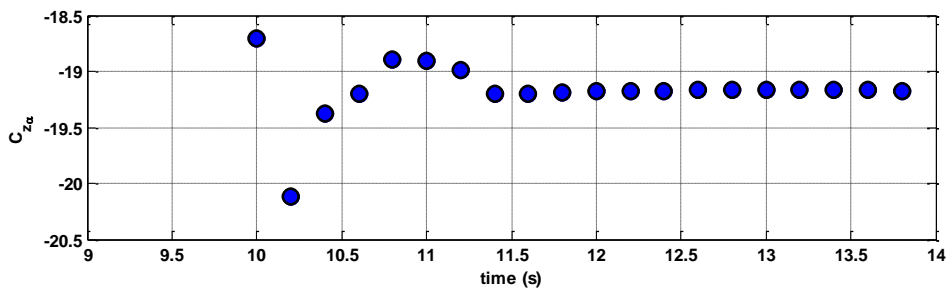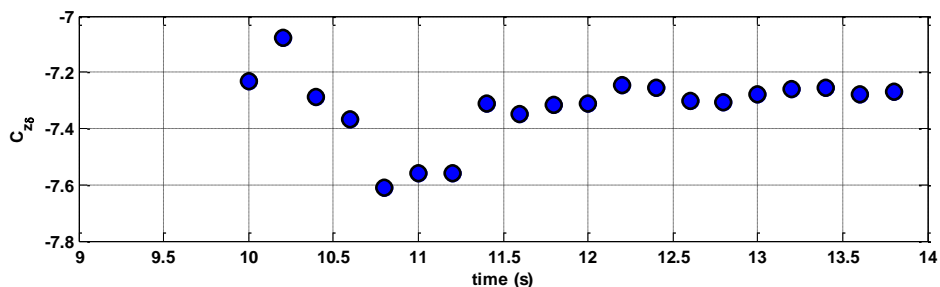


**Figure 3-17 Complex Linear Regression,** $C_{z_\alpha}$



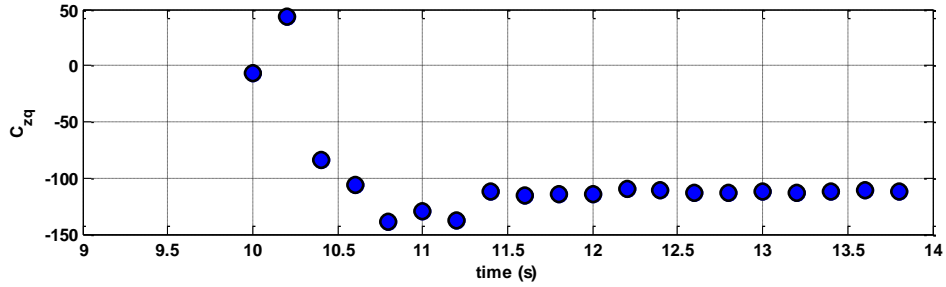**Figure 3-18 Complex Linear Regression,** $C_{z_\alpha}$

**Figure 3-19 Complex Linear Regression,** $C_{z_q}$

As seen from the figure all three model parameters converges about 1 s after SSE input has applied. In addition to that small oscillations remain in the converged data. This is due to at every calculation point a new estimate is done and measurement data is updated with new measurements as missile flights. The numerical comparison between time domain and frequency domain estimation of normal force is also made. The comparison results are given in Table 3-11. The numerical results for complex regression are obtained by averaging after convergence. Note that time domain and frequency domain results are very close.

**Table 3-11 Normal Force Complex Linear Regression Results**

|  | Real Value | Time Domain $\hat{\theta}$ | Frequency Domain $\hat{\theta}$ |
|---|---|---|---|
| $C_{z_\alpha}$ | -19.6295 | -19.187 | -19.18 |
| $C_{z_\delta}$ | -7.41 | -7.2856 | -7.303 |
| $C_{z_q}$ | -113.575 | -112.3293 | -112.9 |

Similar analysis is done for pitching moment. The graphical representation of calculations is given in Figure 3-20, Figure 3-21 and Figure 3-22. As seen from the figures, pitching moment model parameters converge at values again about 1 s after

applying SSE input. In addition to that small oscillations exist like normal force model parameters.
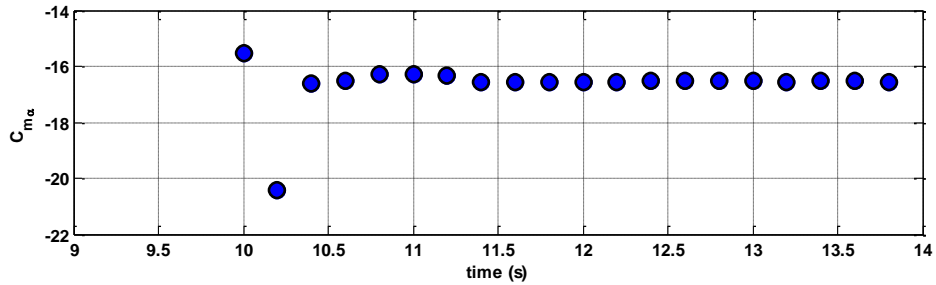


**Figure 3-20 Complex Linear Regression,** $C_{m_\alpha}$



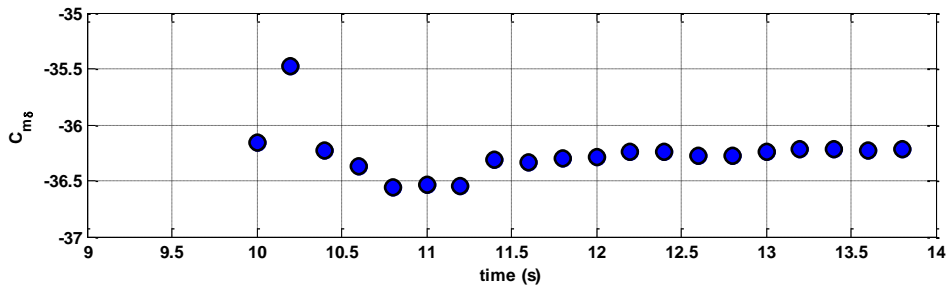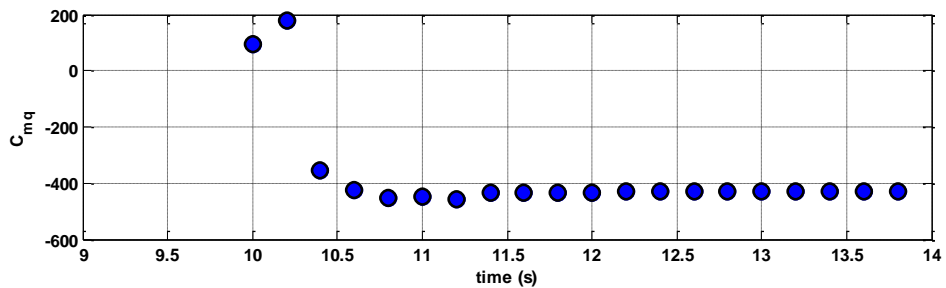**Figure 3-21 Complex Linear Regression,** $C_{m_\delta}$



**Figure 3-22 Complex Linear Regression,** $C_{m_q}$

The numerical comparison between time domain and frequency domain estimation of pitching moment is given in Table 3-12. The numerical results for complex regression are obtained by averaging after convergence. As seen from table the two estimation methods give very close results.

**Table 3-12 Pitching Moment Complex Linear Regression Results**

|  | Real Value | Time Domain $\hat{\theta}$ | Frequency Domain $\hat{\theta}$ |
|---|---|---|---|
| $C_{m_\alpha}$ | -17.544 | -16.5539 | -16.54 |
| $C_{m_\delta}$ | -37.3716 | -36.2128 | -36.24 |
| $C_{m_q}$ | -439.83 | -429.6092 | -430.2 |

## 3.5 Validation with Real Flight Data

In this part of thesis a real flight data collected from an air to ground missile is studied. The main purpose of this part is the validation of the studies given in previous chapters.

Air to ground test missile has a mission computer that calculates acceleration commands for the pre described maneuvers of the missile. The calculated acceleration commands are sent to the autopilot system of the test missile as described in the Section 2.2. The autopilot system is reprogrammed before the test in order to inject SSE to the elevator command. The injected SSE are designed and optimized before the test to collect enough information for parameter estimation. During the flight test all calculated and measured data are sent to a ground station via telemeter system of the test missile.

The collected data from the test missile is classified as confidential so that all the number, graphs are scaled. The scaled data is still meaningful in order to understand that SSE can be used for reduce correlation and open loop parameter estimation from closed loop data.

Square wave SSE is designed for parameter estimation due to ease of programming. Design process is conducted with the procedure given in 3.3.1. During the flight test an acceleration command is applied to the missile whenever excitation input is given to the missile. This is done to increase observability of the states which are used in the estimation process.

### 3.5.1 Data Compatibility Analysis

As mention in Section 2.2.5.2 the position of the inertial measurement must be taken into consideration before conducting parameter estimation. This activity is known as Data Compatibility Analysis. This analysis begins by transferring measurements to the center of gravity of the missile. After transformation process, data used in the parameter estimation process like acceleration, velocity, position etc. must be recalculated. The measurements of an inertial measurement device positioning $r = [x_a y_a z_a]^T$ distance from the center of gravity are corrected as follows.

$$a_{c.g.} = a_{meas} - (w \times r + w \times w \times r) \tag{3-35}$$

Arranging Equation 3-24

$$\begin{bmatrix} a_x \\ a_y \\ a_z \end{bmatrix}_{c.g.} = \begin{bmatrix} a_x \\ a_y \\ a_z \end{bmatrix}_{ölçüm} + \begin{bmatrix} (q^2 + r^2) & -(pq - \dot{r}) & -(pr + \dot{q}) \\ -(pq + \dot{r}) & (p^2 + r^2) & -(qr - \dot{p}) \\ -(pr - \dot{q}) & -(qr + \dot{p}) & (p^2 + q^2) \end{bmatrix} \begin{bmatrix} x_a \\ y_a \\ z_a \end{bmatrix} \tag{3-36}$$

The corrected z acceleration measurement of the test missile is shown Figure 3-23. Note that transformed signal differs from measured signal. That change effect directly estimation results.
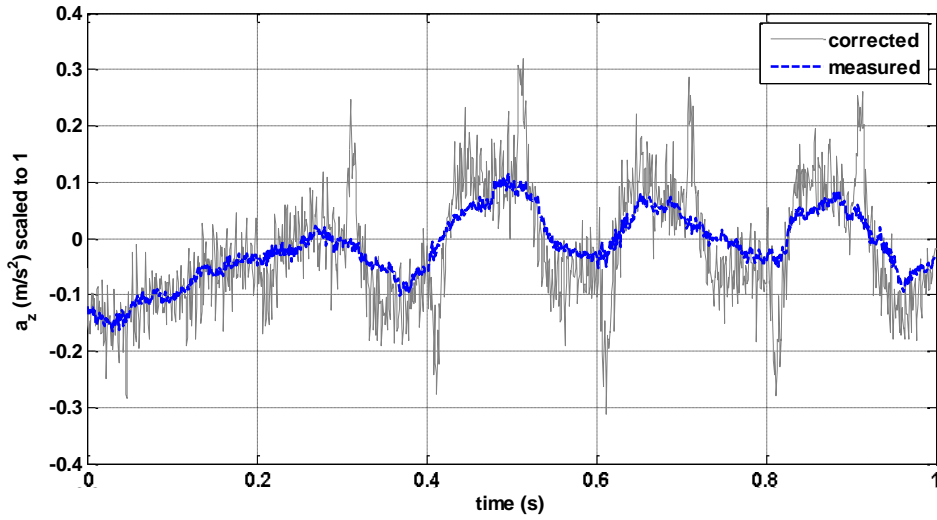
**Figure 3-23 Test Missile z force**

## 3.5.2 Flight Test Parameter Estimation Results

For the analysis of test missile static part of aerodynamic model equations defined in Equation 3-1 and 3-2 are used. The model structure for z force and pitching moment are given in Equation 3-38 and 3-39.

$$C_z = C_{z_0} + C_{z_\alpha}\alpha + C_{z_\delta}\delta \tag{3-37}$$

$$C_m = C_{m_0} + C_{m_\alpha}\alpha + C_{m_\delta}\delta \tag{3-38}$$

The static aerodynamic parameters are estimated using ordinary least squares defined in section 3.1. The estimation result for the z force and comparison with aerodynamic database is given in Figure 3-24 and Table 3-13. Figure 3-24 shows Least Squares Model Fit for first portion of the flight test. As seen from the figure model fit is good enough to estimate z force parameters. The residual figure has almost normal distribution which shows the model structure defines the behavior of the missile very well.
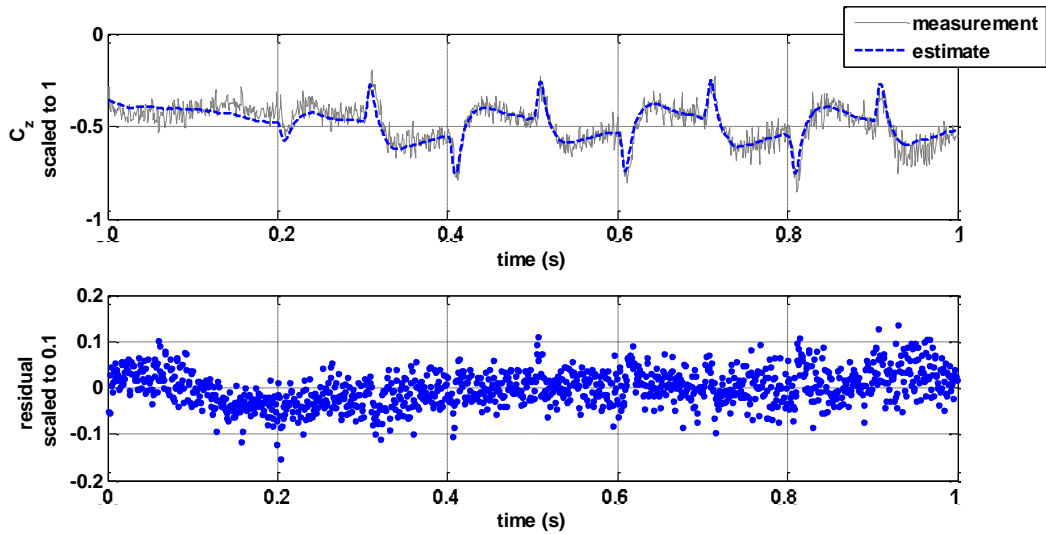
74

**Figure 3-24 Least Squares model fit to $C_z$ and residuals, Flight Test**

The values of estimation results are summarized in Table 3-13. As seen from the results, $C_{z_\alpha}$ estimate values are very close to the aerodynamic database. The error is about % 10. On the contrary the errors for $C_{z_\delta}$ values are about % 14. This condition may come from that inadequate SSE input design or from the inaccurate aerodynamic database.

**Table 3-13 Least Squares parameter estimation results, $C_z$, Flight Test**

|  | Real Value | $\hat{\theta}$ | $s(\hat{\theta})$ | $|t_0|$ | $s(\hat{\theta})/|\hat{\theta}|$ | $s = \hat{\sigma}$ | $R^2$ | Correlation |
|---|---|---|---|---|---|---|---|---|
| $C_{z_\alpha}$ | -1 | -1.086 | 0.006 | 36.702 | 2.725 | 0.076 | %75.4 | 0.317 |
| $C_{z_\delta}$ | -1 | -0.863 | 0.002 | 35.610 | 2.808 | 0.076 | %75.4 | 0.317 |

The estimation analysis for the normal force is repeated for the pitching moment. The results are given in Figure 3-25 and Table 3-14. Like z force estimation Figure 3-25 shows the model fit for the first portion of the flight test. As seen from the figure the model structure suits well to the measurement. The residuals distributed almost normally.
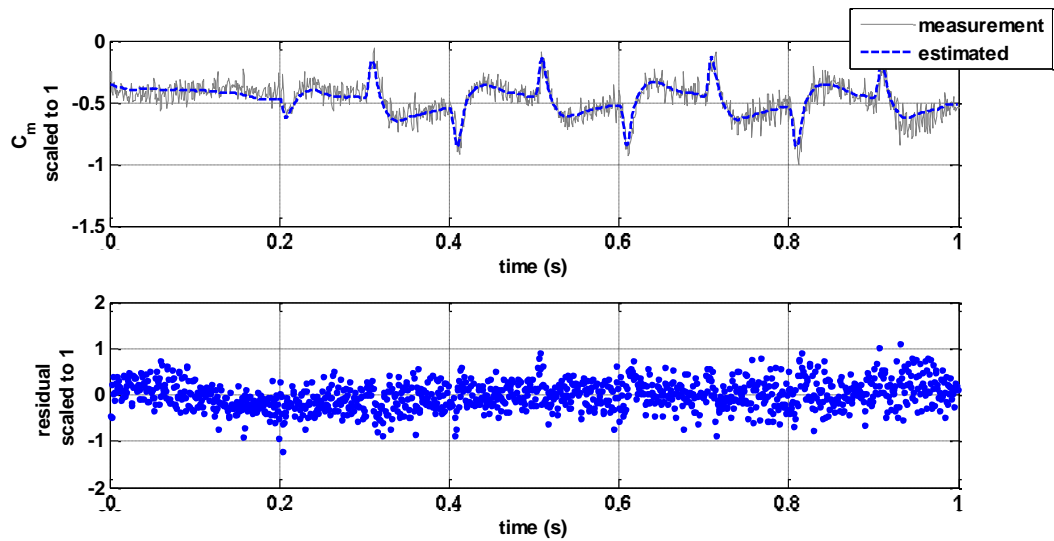
**Figure 3-25 Least Squares model fit to $C_m$ and residuals, Flight Test**

As seen from Table 3-14 the $C_{m_\alpha}$ estimate values are very close to the aerodynamic database. The error is about % 10 which is acceptable. On the contrary the errors for $C_{m_\delta}$ values are about % 16 like the errors for z force. These errors come from inadequate input design or inaccurate aerodynamic database as mentioned before.

**Table 3-14 Least Squares parameter estimation results, $C_m$, Flight Test**

|  | Real Value | $\hat{\theta}$ | $s(\hat{\theta})$ | $|t_0|$ | $s(\hat{\theta})/|\hat{\theta}|$ | $s = \hat{\sigma}$ | $R^2$ | Correlation |
|---|---|---|---|---|---|---|---|---|
| $C_{m_\alpha}$ | -1 | -1.098 | 0.049 | 27.607 | 3.622 | 0.607 | %73 | 0.317 |
| $C_{m_\delta}$ | -1 | -0.838 | 0.020 | 39.696 | 2.519 | 0.607 | %73 | 0.317 |

# CHAPTER 4

# CONCLUSION

Parameter estimation results are widely used for several purposes such as verifying and improving computational and wind-tunnel test results, developing flight simulations in large flight regimes, investigating stability and control impact of airframe modifications. For unstable configuration or stable configuration with feedback control brings new challenges in the parameter estimation field. New techniques or new input design must be studied for open loop parameter estimation from closed loop data.

In this thesis design of SSE is studied to solve the challenges of parameter estimation from closed loop data. The study is done in Section 3.3. A stacked sine wave is selected with a systematic manner. The effect of amplitude and frequency to the collinearity is also showed. According to study the signals that excite the system near natural airframe frequencies gives best data collinearity result which affect directly estimation results.

In Section 3.4 parameter estimation study using ordinary least squares is done. The SSE signal is selected according to the analysis done in previous section. The estimation process is done using noisy measurements. The results are acceptable comparing with real value of parameters computed from aerodynamic database. The success of SSE input in parameter estimation field is shown which one of the aims of the thesis is.

In Section 3.4.2 the estimation process is studied in the frequency domain. The main purpose of this study to show that parameter estimation using SSE can be done in

near real-time. In addition to that both time domain and frequency domain technique are compared each other.

In Section 3.5 the work done in Section 3.3 and 3.4 are validated by real flight data. Parameter estimation is done using flight test result of an air to ground test missile. The missile excited using square wave SSE signals and parameters are estimated using ordinary least squares. The estimation results are compared with test missile aerodynamic database. The results are acceptable which shows that SSE can easily be used to reduce data collinearity and open loop parameter estimation.

The following items are listed as recommendations for future works.

By studying near real time parameter estimation using SSE aerodynamic stability and control derivatives can be fed to an adaptive controller. So that control authority can be reconfigured near real time in possible failure conditions such as damaged control surface in air.

The investigation of input signals can be expanded. So that a wide range of mixed signals and their effect to data collinearity and parameter estimation can be investigated.

# REFERENCES

1] Klein V., Morelli E. A., "Aircraft System Identification Theory and Practice" 2006

[2] Jategaonkar R., "Flight Vehicle Identification: A Time Domain Methodology" 2006

[3] Hamle P. G., Jategaonkar R. V., "The Role of System Identification for Flight Vehicle Applications - Revisited" RTO held in Madrid, Spain, 5-7 May 1998,

[4] Hamel P. G., "Aircraft Parameter Identification Methods and Their Applications - Survey and Future Aspects", AGARD LS-104, Nov. 1979, Paper I

[5] Mulder J. A., Jonkers, H. L., Horsten, J. J.,Breeman, J. H., and Simon, J. L., "Analysis of Aircraft Performance, Stability and Control Measurements", AGARD LS-104, Nov. 1979, Paper 5.

[6] Maine R. E. and Iliff, K. W., "Identification of Dynamic Systems", AGARD AG-300, Vol. 2, Jan. 1985.

[7] Klein V., "Estimation of Aircraft Aerodynamic Parameters from Flight Data" Progress in Aerospace Sciences, Pergamon Press, Oxford, Vol. 26, 1989, pp. I-77

[8] Klein V., "Application of System Identification to High Performance Aircraft" Proceedings of the 32nd IEEE Conference on Decision and Control, San Antonio, TX, December 1993, pp. 2253-2259

[9] Klein V., Murphy, P. C., "Aerodynamic Parameters of High Perfomance Aircraft Estimated from Wind Tunnel and Flight Test Data" System Identification for Integrated Aircraft Development and Flight Testing, NATO Res. And Techn. Org., RTO-MP-11, Paper 18, May 1999

[10] Weiss S., Friehmelt H., Plaetschke E., Rohlf D., "System Identification Using Single-Surface Excitation at High Angles of Attack" AIAA-1995-

3436, AIAA Atmospheric Flight Mechanics Conference, Baltimore, MD, August 1995

[11]   Moes, T.R., Smith, M.S., and Morelli, E.A.   "Flight Investigation of Prescribed Simultaneous Independent Surface Excitations (PreSISE) for Real-Time Stability and Control Derivative Estimation,"  AIAA-2003-5702, AIAA Atmospheric Flight Mechanics Conference, Austin, TX, August 2003. Re-published as NASA/TM-2003-212029, October 2003

[12]   Morelli E. A., "Multiple Input Design for Real-Time Parameter Estimation in the Frequency Domain" 13th WAC Conference on System Identification August 27-29,2003 / Rotterdam, The Netherlands

[13]   Baumann E., "Tailored Excitation for Frequency Response Measurement Applied to the X-43A Flight Vehicle", NASA/TM-2007-214609

[14]   Reagan C. D., "In-Flight Stability Analysis of the X-48B Aircraft" AIAA-2008-6571, AIAA Atmospheric Flight Mechanics Conference and Exhibit, Honolulu, HI, August 2008

[15]   Holzel M. S., Morelli E. A., "Real-Time Frequency Response Estimation from Flight Data", AIAA 2011-6358, AIAA Atmospheric Flight Mechanics Conference 08 - 11 August 2011, Portland, Oregon

[16]   http://www.navy.mil/navydata/fact_display.asp?cid=2200&tid=200&ct=2

[17]   http://en.wikipedia.org/wiki/Harpoon_(missile)

[18]   http://www.boeing.com/defense-space/missiles/harpoon/docs/HarpoonBlockIIBackgrounder.pdf

[19]   http://www.boeing.com

[20]   Avcıoğlu H.T., "A tool for trajectory planning and performance verification of cruise missiles" 2000

[21]   MIL HDBK 1211 NOT 1 Missile Flight Simulation

[22]   International Organization for Standardization, Standard Atmosphere, ISO 2533:1975, 1975

[23]   The international system of units (SI) − United States Department of Commerce, NIST Special Publication 330, 2008, p. 57

[24]   Bruns, K. D., MISSILE DATCOM User's Manual - Revision 6/93